

RESEARCH ARTICLE

A Spiral Coverage Path Planning Algorithm for Nonomnidirectional Robots

Taogang Hou¹  | Jiaxin Li¹ | Xuan Pei¹ | Hao Wang² | Tianhui Liu¹

¹Institute of Advanced Control Systems, School of Automation and Intelligence, Beijing Jiaotong University, Beijing, China | ²Institute of Robotics, School of Mechanical Engineering and Automation, Beihang University, Beijing, China

Correspondence: Taogang Hou (houtaogang@bjtu.edu.cn)

Received: 15 April 2024 | **Revised:** 23 October 2024 | **Accepted:** 5 January 2025

Funding: The study was supported by Young Elite Scientists Sponsorship Program by CAST (Grant No. 2022QNRC001), National Natural Science Foundation of China (Grant No. 62103035), Beijing Natural Science Foundation (Grant Nos. 3222016 and L231004).

Keywords: complete coverage path planning | coverage efficiency | high-coverage-rate turning strategy | nonomnidirectional robot | path planning | robotics | spiral coverage path

ABSTRACT

The limited steering capabilities of nonomnidirectional robots introduce significant complexity into complete coverage tasks, often leading to increased path overlap or incomplete coverage of certain areas. Although recent research has made progress in optimizing coverage path planning, redundant coverage or omissions are still prone to occur in the target area to be covered. To address these persistent challenges, we propose a novel spiral coverage method. This approach not only conforms to the kinematic constraints of nonomnidirectional robots but also enhances coverage efficiency by dividing the target area into center and boundary regions and devising tailored coverage strategies for each. This method effectively reduces path redundancy and improves overall area coverage. Furthermore, we introduce a comprehensive metric that combines total path length and area coverage ratio to evaluate coverage efficiency, overcoming the limitations and computational complexity associated with existing metrics. For scenarios where maximizing the area coverage ratio is critical, we have developed a high-coverage-rate turning strategy that ensures 100% coverage. Through simulation tests in six representative areas and actual experiments on airport runways, our method shows an improvement of 0.238%–14.538% in coverage efficiency compared with parallel coverage method and 60.548%–76.339% compared with deep reinforcement learning-based method. Additionally, implementing high-coverage-rate turning strategies improves the area coverage ratio by 2.021%–6.732%. In field experiments, our method reduces execution time by 1.61% compared with parallel coverage method. These results show that our method has a significant effect in improving coverage efficiency and achieving complete coverage goals.

1 | Introduction

Complete coverage path planning (CCPP) is a fundamental task in robotics, aiming to ensure that every point within a specified area is covered efficiently so that the robot can maximize comprehensive information acquisition or task execution. This has led to the widespread application of CCPP in various fields, including three-

dimensional printing (Zhao et al. 2016), lawn mowing (Hameed 2017), agricultural harvesting (Pour Arab, Spisser, and Essert 2023; Höffmann, Patel, and Büskens 2024; Oksanen and Visala 2009), indoor cleaning (Lakshmanan et al. 2020; Engelsons, Tiger, and Heintz 2022; Bormann et al. 2016; Liu, Ma, and Huang 2018), bush trimming (Kaljaca, Vroegindeweij, and van Henten 2019), and area patrolling (Luis, Reina, and Marín 2020). One of the key challenges

Jiaxin Li and Taogang hou are first co authors.

in CCPP arises from the diversity of robotic platforms, each with its own set of mobility constraints and operational requirements. Particularly, nonomnidirectional robots face constraints in their turning radius, complicating path planning (Xu et al. 2009), as depicted in Figure 1a. These robots require smooth paths that satisfy kinematic constraints, rather than segmented polylines, to ensure feasible execution. Failing to account for these kinematic constraints during path planning can render the paths infeasible, leading to ineffective navigation or collisions with environmental obstacles. Various methods have been developed to address this challenge, including learning-based methods and two traditional methods: parallel strip coverage and spiral coverage.

Learning based CCPP methods have gained attention in recent years due to their high degree of automation and strong adaptability to complex and dynamic environments. Reinforcement learning algorithms, such as Q-Learning and Deep Q-Networks (DQN), enable robots to plan paths through interaction with their environments, performing well in dynamic and unknown settings. Literature (Tan et al. 2023; Piardi et al. 2019; Carvalho and Aguiar 2023) have demonstrated the effectiveness of these methods in managing dynamic environments and unknown maps. However, in large environmental maps, sparse learning rewards can significantly slow down the convergence speed of the Q-function, sometimes preventing convergence altogether, which can result in poor path continuity and consistency. Zhang, Cai, and Pang (2023) addressed this by introducing a smoothness reward function to improve path continuity and comply with kinematic constraints. Similarly, Jonnarth, Zhao, and Felsberg (2023) proposes an online CCPP method based on continuous end-to-end deep reinforcement learning, achieving efficient coverage in unknown environments using multi-scale frontier maps and total change reward mechanisms. However, in known environments such as agricultural fields and residential cleaning areas, learning-based methods might not perform optimally as they may generate excessive exploratory paths, leading to inefficiencies. In contrast, traditional algorithms that can provide more direct and efficient paths without the need for exploration. Additionally, learning-based methods typically require extensive high-quality training data, which can be resource-

intensive and time-consuming to obtain and label. These methods may also struggle to generalize to new environments that differ significantly from the training data.

Traditional methods hold a significant position in the field of CCPP due to their stability, reliability, and lower computational costs. These methods continue to be widely applied and actively researched. Based on path patterns, they can be categorized into parallel strip coverage methods and spiral coverage methods. The parallel strip coverage methods mostly utilize the headland pattern (Bochtis and Vougioukas 2008; Evans IV et al. 2020; Zhou et al. 2014), as illustrated in Figure 1b. This method requires determining whether the headland region can be set outside the coverage area or whether it must be located within the coverage area. If the space outside the coverage area is large enough, the headland region is set outside the coverage area; otherwise, it must be within the coverage area. The headland region is typically used for robot turning, while the non-headland region is divided into a series of parallel strips that the robot traverses to cover the area (Bochtis and Vougioukas 2008). When the headland region is located outside the coverage area, only the non-headland region requires coverage. Efficient coverage of the nonheadland region can be achieved by minimizing the total nonworking path length within the headland region. Literature (Bochtis and Vougioukas 2008; Bochtis, Vougioukas, and Griepentrog 2009; Evans IV et al. 2020; Conesa-Muñoz, Pajares, and Ribeiro 2016; Jensen et al. 2012; Bochtis, Sørensen, and Vougioukas 2010; Bakhtiari et al. 2011) have optimized the shortest nonworking path coverage by framing it as a traversal over a weighted graph, determining an optimal traversal sequence equivalent to the shortest path within the graph. However, these methods may not generalize well to scenarios where the headland region is within the coverage area, as they leave many uncovered regions. Research (Nilsson and Zhou 2020a, 2020b) has addressed the issue of large uncovered areas by using spiral paths in the headland region. But due to constraints on the robot's turning radius, some areas at the turns of the spiral path remain uncovered, as shown in Figure 1c. Further improvements in coverage rates have been

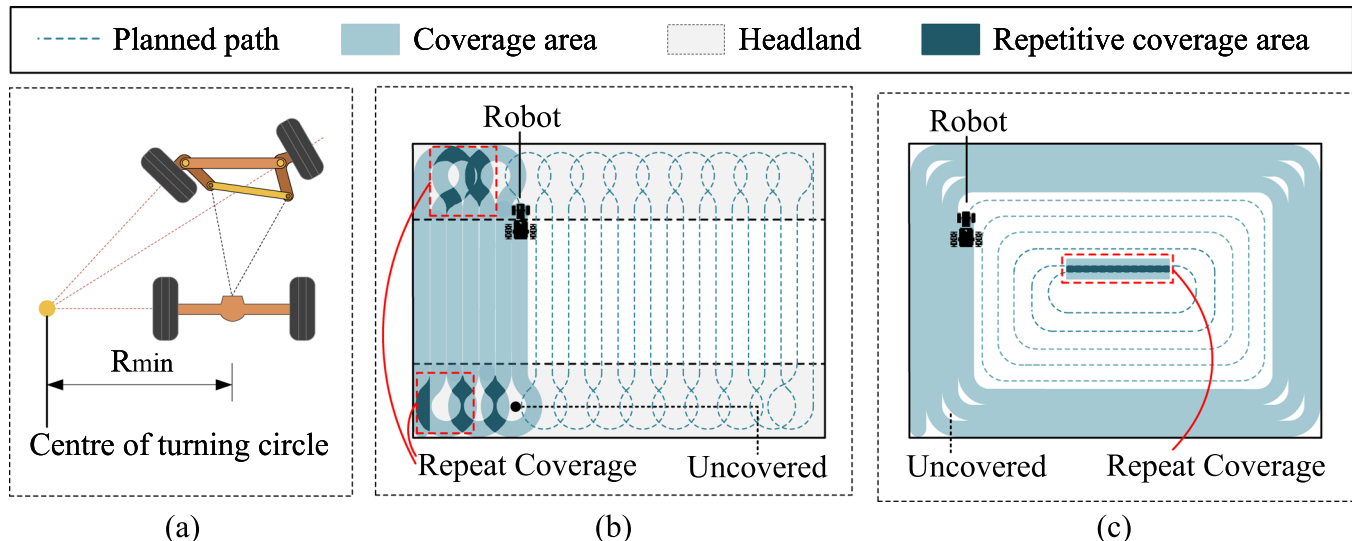


FIGURE 1 | (a) Steering structure of nonomnidirectional robots. (b) Headland pattern coverage path. (c) Spiral coverage path. [Color figure can be viewed at wileyonlinelibrary.com]

achieved by refining the turning strategy of spiral paths within the headland region (Zhang et al. 2022; Jeon et al. 2021; Edwards et al. 2017). Although introducing spiral paths into the headland region of the parallel strip coverage methods improves the area coverage rate, there will be a large number of overlapping coverage paths between the original turning paths and the newly added spiral paths in the headland region, resulting in a decrease in overall coverage efficiency.

Unlike the limited use of spiral paths within the headland regions of parallel strip coverage methods, the spiral coverage method primarily employs a continuous spiral path to cover the entire target area. This method involves the robot following a trajectory that loops around the target area, progressively moving either outward from the center (inside-out) or inward toward the center (outside-in). Spiral coverage paths offer several advantages over parallel strip coverage paths. Firstly, they allow the robot to navigate at higher speeds without introducing additional wheel slip (Khan, Noreen, and Habib 2017; Bosse, Nourani-Vatani, and Roberts 2007; Choi et al. 2009). In parallel coverage paths, the presence of 180° turns requires the robot to change its velocity direction four times, considering a nonzero minimum turning radius. In contrast, spiral coverage paths involve turns with angles consistently smaller turns, requiring only two direction changes, which reduces both the frequency of velocity adjustments and the potential for slippage. Secondly, spiral coverage paths keep the work area always on the same side of the robot, which can improve localization accuracy. In parallel coverage paths, the robot switches direction every time it moves to a new parallel strip path, which can negatively impact localization. However, despite these advantages, spiral coverage also has shortcomings when applied to nonomnidirectional robots. As the spiral path approaches the center of the area, the remaining uncovered regions become progressively smaller, resulting in inevitable overlap when the robot turns within the central region, as shown in Figure 1c. Therefore, ensuring that spiral coverage paths meet the kinematic constraints of nonomnidirectional robots while minimizing overlaps remains a significant challenge.

Having discussed various CCPP methods, it is crucial to accurately evaluate the actual performance of these methods. To compare the effectiveness of these CCPP methods, commonly employed metrics include total path length (*TPL*) and area coverage ratio (*ACR*). *TPL* measures the length of the coverage path, while *ACR* reflects the proportion of the designated area that is covered. However, these individual metrics have certain limitations. Evaluating algorithms based solely on *TPL* tends to favor shorter paths, which might not achieve comprehensive area coverage. On the other hand, when the *ACR* is used to evaluate the algorithm, sufficiently long paths enable the robot to continue exploring the target area to achieve complete coverage, but excessively long paths will notably decrease the robot's work efficiency. Therefore, neither the *TPL* nor the *ACR* can comprehensively evaluate the performance of the algorithm. It becomes necessary to design suitable evaluation metrics for efficiency. Some studies (Bakhtiari et al. 2011; Zhai et al. 2021) have utilized metrics like the effective path ratio to evaluate efficiency, but these metrics are limited to parallel coverage algorithms in situations where headland region is set outside the coverage area. In this case, the effective path length is equal to the sum of the lengths of the parallel strips and the ineffective path length is equal to the sum of the lengths of the steering paths in the headland region. However, the computation of the effective path length

becomes more difficult in the situations where the headland region is within the coverage area.

In this study, an offline CCPP method tailored for nonomnidirectional robots operating within various polygonal environments is proposed. The universal adaptation of this method stems from the nature of polygonal regions, which can be decomposed into multiple convex polygons or approximated as a single convex polygon using specific techniques (McClure and Vitale 1975; De Berg 2000; o'Rourke 1998; Keil and Sack 1985). This method generates paths that spiral inward from the boundary of the target area to be covered. To maintain consistency with descriptions used in related research (Gonzalez et al. 2003; Gabriely and Rimon 2002), we refer to our method as the Spiral Coverage Path Planning Algorithm. The contributions of this paper are as follows:

- 1 Proposed a spiral coverage method: This method divides the target coverage area into boundary and center regions for separate coverage. The boundary region is covered using a spiral path, which do not generate overlapping; in the center region, two steering paths with low overlap rates are designed, namely “T-shaped” and “Ω-shaped” steering paths. Solved the problem of existing spiral CCPP algorithms not meeting the kinematic constraints of robots and have a high overlap rate in the center region. The proposed spiral coverage method is more stable, reliable, and cost-effective compared to learning-based method, achieving 60.548%–73.777% higher coverage efficiency, and it outperforms traditional parallel stripe coverage method with an efficiency improvement of 0.238%–14.538%.
- 2 High-coverage-rate turning strategy: We proposed a high-coverage-rate turning strategy that effectively addresses partially uncovered areas at the turns of the spiral path. This strategy enables 100% area coverage, ensuring no part of the target area is missed. It is particularly valuable in applications requiring strict full coverage, such as demining operations (ensuring no areas are left unchecked for safety) and clean-room maintenance in semiconductor manufacturing (maintaining strict hygiene standards by covering all areas).
- 3 Comprehensive evaluation metric: To solve the problem that existing evaluation metrics cannot comprehensively evaluate path coverage efficiency (*TCE*) or are difficult to calculate in certain scenarios, we combined *TPL* and *ACR* to design a widely applicable and effective efficiency evaluation metric.

Our proposed spiral coverage path demonstrates high coverage efficiency, making it particularly advantageous in outdoor scenarios where robots cannot recharge frequently. For instance, in agricultural harvesting or cleaning large open areas, our method covers more area with shorter paths, enhancing efficiency. The combination of our spiral path and high-coverage-rate turning strategy ensures 100% coverage, making it ideal for scenarios requiring strict complete coverage. This is especially critical in hospital floor disinfection, where maintaining hygiene and safety standards is paramount, or in industrial inspection and maintenance, where thorough coverage of critical infrastructure is necessary to identify potential issues. Furthermore, in smart manufacturing, our method can ensure comprehensive coverage for tasks such as floor cleaning and inspection, contributing to a cleaner and safer production environment. In service robots, especially those deployed in large facilities or public spaces, our approach ensures that areas are

thoroughly covered, improving service quality and user satisfaction. By addressing the limitations of existing methods and introducing innovative solutions, our spiral coverage algorithm demonstrates significant improvements in both efficiency and applicability across a range of environments and applications, including agriculture, industrial maintenance, smart manufacturing, and medical facilities.

The rest of this article consists of the following: In Section 2, a review is conducted on the challenges faced by the CCPP algorithms for nonomnidirectional robots. In Section 3, the proposed spiral CCPP algorithm, the high-coverage-rate spiral turning strategy and efficiency evaluation metric are introduced. Section 4 presents experiments designed to validate the proposed algorithm and compare it with traditional path planning methods and deep reinforcement learning-based method. Finally, Section 5 outlines the main conclusions of this study.

2 | Related Works

In this section, we review key developments in CCPP, focusing on three critical aspects: spiral path planning algorithms, efficiency evaluation metrics, and turning strategies for spiral paths. These aspects represent major challenges in the field and highlight opportunities for further innovation. By examining recent advancements, we aim to provide a comprehensive overview of the current state of research and identify areas for future improvement.

2.1 | Spiral Coverage Path Planning Algorithm

Spiral coverage path planning involves generating paths by following either an inside-out or outside-in spirals, depending on the environment and task requirements. Literature (Cabreira et al. 2018) proposed an algorithm for generating inner spiral paths within a polygonal region, primarily designed for UAV photogrammetry applications. This algorithm, however, does not consider kinematic constraints, which limits its applicability to ground robots. For nonomnidirectional robots, Bosse, Nourani-Vatani, and Roberts (2007) introduced a spiral path planning algorithm tailored for outdoor, unstructured environments. Their approach generates translational spiral paths to address coverage issues at the center of the target region. However, the paths created by the translational spiral operation still suffers from redundant coverage, as certain areas are covered multiple times. The challenge of reducing overlapping coverage and improving overall area coverage remains unsolved. Inspired by the literature. Inspired by the literature (Bosse, Nourani-Vatani, and Roberts 2007), we design the spiral path planning method for target region coverage and propose two novel coverage methods for center region coverage, which have less overlapping coverage areas than the translational spiral path.

2.2 | Efficiency Evaluation Metrics

Given the prevalence of overlapping path coverage in many existing coverage path planning algorithms, the degree of overlapping coverage to some extent indicates the efficiency of the algorithm. Therefore, there is an obvious need for specialized evaluation metrics to assess algorithmic efficiency. Literature (Seyyedhasani,

Dvorak, and Roemmle 2019; Seyyedhasani and Dvorak 2018a, 2018b; Grisso et al. 2004) employs field efficiency for assessing the efficiency of farmland mulching operations. This metric primarily considers only the actual operating time and total time, without factoring in path coverage. Literature (Lee et al. 2010; Cao et al. 2019; Zhou et al. 2020; Hameed, Bochtis, and Sorensen 2011) employs overlap ratio to represent algorithm efficiency. However, the overlap ratio only focuses on the degree of path repetition and does not consider the time or path length required for the robot to complete the full coverage task. Consequently, in some cases, although the path overlap ratio is low, the time required to complete the task may be longer. Overall, existing evaluation metrics for CCPP algorithms fail to comprehensively assess algorithm efficiency. Therefore, we propose new evaluation metric that combine total path length and area coverage ratio, aiming for a more comprehensive assessment of efficiency.

2.3 | Turning Strategies for Spiral Paths

In many coverage path planning approaches, particularly those employing parallel coverage strategies, the primary focus lies on scenarios where the headland region is located outside the area to be covered, meaning only the non-headland areas need to be covered, and the headland region can be ignored. However, in real-world applications such as robotic inspections or indoor cleaning tasks, comprehensive coverage of the entire designated area is often required. In such cases, the headland region is typically located within the area to be covered and cannot be ignored. Recognizing this discrepancy, researchers have sought alternative methodologies to ensure full-area coverage. One notable solution proposed in literature (Nilsson and Zhou 2020a, 2020b) involves using spiral paths to cover the headland region. By incorporating spiral paths specifically within the headland area, this method effectively extends coverage to previously neglected areas, thereby enhancing the completeness of the coverage path. Although spiral paths within the headland region have proven effective in enhancing coverage, challenges persist, particularly with inadequate coverage at the turning points of these spiral paths. Zhang et al. (2022); Jeon et al. (2021); Edwards et al. (2017) introduces a novel turning strategy, whereby a short segment of the path is generated along the original direction before turning, followed by retracing the path back to the turning point to generate the turning path. While this strategy represents progress in improving area coverage, it is crucial to note that complete coverage may still not be achieved, underscoring the need for further refinement in the design of turning strategies.

3 | Methods

To achieve complete coverage in an arbitrary area, two approaches can be considered: decomposition into multiple convex polygonal regions or approximation as a convex polygonal region using appropriate approximation methods. These methods allow us to focus on the study of complete coverage of convex polygons. Spiral coverage path planning involves creating a continuous spiral path by gradually offsetting inward from the boundary of the area to be covered. Compared with traditional parallel coverage paths, spiral coverage paths can reduce coverage duplication to some extent. When considering the turning radius constraints of robots, planning spiral coverage paths remains an urgent issue. As the uncovered

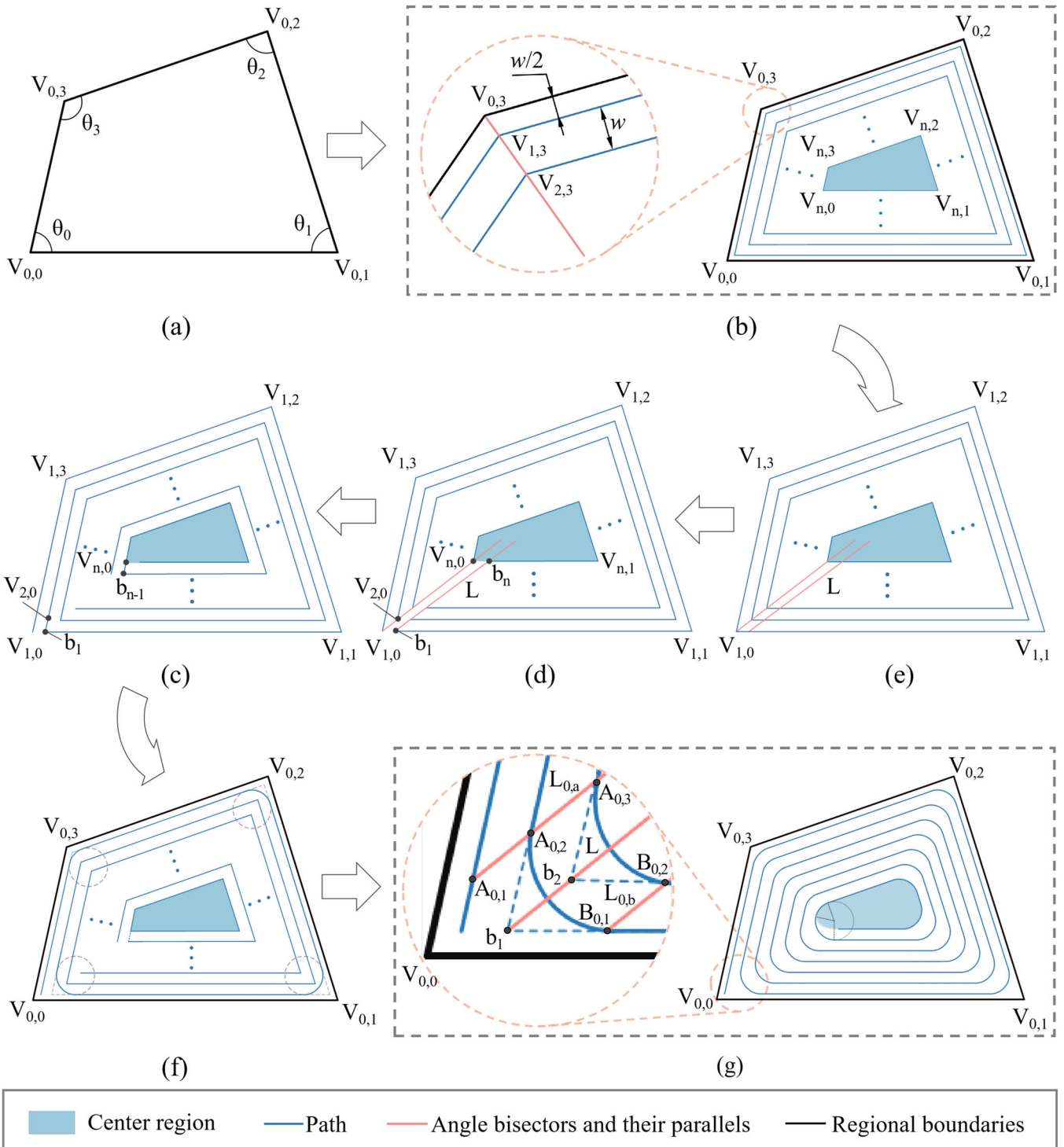


FIGURE 2 | Schematic of the spiral path generation process in the boundary area. (a) the input quadrilateral area to be covered; (b) generation of contour-parallel paths; (c), (d), (e) the process of transforming from contour-parallel paths to spiral path; (f) the smoothing process of polyline spiral paths using circular arcs; (g) the complete smooth spiral coverage path generated within the boundary region. [Color figure can be viewed at wileyonlinelibrary.com]

region decreases during the coverage process, the remaining region near the center will no longer provide a steerable region for the robot without generating overlaps, as shown in Figure 2g. To mitigate path overlapping and ensure that the planned paths satisfy the kinematic constraints of the robot, we propose an algorithm that divides the area to be covered into a boundary region and a center region and designs different paths to cover them. The boundary

region provides sufficient space for the robot to make turns, and the path generated within the boundary region comply well with the minimum turning radius restriction of the robot. However, due to the relatively small size of the center region, it becomes challenging to generate spiral paths that satisfy the turning radius constraint within this area. Therefore, we propose two coverage paths suitable for the center region. In the following sections, the method of

generating spiral path in the boundary region and the methods of generating coverage paths in the center region will be detailed using a convex quadrilateral as an example. These methods, while exemplified with a quadrilateral, are equally applicable to more complex polygonal shapes. Additionally, a metric for evaluating coverage efficiency is introduced, and a coverage area calculation model for the spiral coverage algorithm is established to quantify the relationship between the coverage area and the parameters of robot. Moreover, a steering strategy with high coverage rate is designed to address full coverage.

3.1 | Spiral Coverage Path Generation

3.1.1 | Modeling of the Coverage Area

First, set the coordinates of the four vertices of the quadrilateral area to be covered, as well as the robot's minimum turning radius, denoted as R_{min} , and the robot's coverage width, denoted as w . As shown in Figure 2a, label the four vertices of the quadrilateral in a counterclockwise direction as $V_{0,0}, V_{0,1}, V_{0,2}, V_{0,3}$. Similarly, label the four internal angles in a counterclockwise direction as $\theta_0, \theta_1, \theta_2, \theta_3$. The edge $V_{0,0}V_{0,1}$ is the longest side of the quadrilateral.

3.1.2 | Coverage Method for the Boundary Region

3.1.2.1 Generation of Contour-parallel Paths

After defining the work area to be covered, the boundary lines are biased inward to generate contour-parallel paths. As shown in Figure 2b, considering the robot's coverage width, the first contour-parallel path should be generated with a width of $w/2$ from the area boundary. This means that the first contour-parallel path is obtained by moving each edge of the input quadrilateral inward by a distance of $width_1 = w/2$. The n -th contour-parallel path further on is obtained by intersecting each edge of the first contour-parallel path after inwardly shifting it by a certain distance $width_n = (n - 1)w$, (where n is the index of the contour-parallel path, and $n > 1$). According to the property of the angle bisector, which states that the points on the angle bisector are equidistant from both edges of the angle, it can be known that the vertices of the contour-parallel paths are located on the angle bisector of θ_i , and the vertices of the contour-parallel paths are denoted by $V_{n,i}$, where i denotes the index of the vertices of the quadrilateral region, arranged counterclockwise starting from the vertex $V_{0,0}$, with i ranging from 0 to 3. The distance between the vertices $V_{1,i}$ of the first contour-parallel path and the vertices $V_{0,i}$ of the work area is given by

$$d_i = \frac{w}{2 \sin\left(\frac{\theta_i}{2}\right)}. \quad (1)$$

The distance between the vertices $V_{n,i}$ (where $n \geq 2$) of the n -th contour-parallel path and the vertices $V_{1,i}$ is given by

$$d_i = (n - 1) \frac{w}{\sin\left(\frac{\theta_i}{2}\right)}, (n \geq 2). \quad (2)$$

The contour-parallel paths obtained at this time are disconnected from each other.

3.1.2.2 Connecting contour-parallel paths to obtain spiral path

In the previous step, the contour-parallel paths obtained are independent of each other, necessitating further processing to connect them. Here, we set vertex $V_{1,0}$ as the starting point to generate a clockwise path. The angle bisector of θ_0 is shifted to the right by a distance $x = w/\sin(\theta_0)$ to create line L, as shown in Figure 2e. The intersection of the straight line L with the parallel edge $V_{n,0}V_{n,1}$ (where $n \geq 1$) is set to interrupt the point b_n . Then the point $V_{n,0}$ is disconnected from the point b_n , as shown in Figure 2d. By connecting point $V_{n,0}$ to point b_{n-1} (where $n \geq 2$), a spiral path is formed as shown in Figure 2c.

3.1.2.3 Smoothing the spiral path

The obtained spiral path is composed of multiple connected polyline segments. Due to the nonholonomic structure and limited maneuverability of nonomnidirectional robots, they are unable to rapidly change direction. This limitation also prevents them from executing polyline paths. Therefore, to ensure that the planned path can be executed by the robots, it is necessary to smooth the spiral path. This is achieved by using circular arcs to smooth the polyline segments. As illustrated in Figure 2f, the centers of the articulated arcs are located on the angle bisectors of θ_i , and the radii of the arcs are equal to the smallest turning radius of the robot. Instead of moving the center of a circle with a radius of R_{min} along the angle bisector to intersect with the polyline segments to find the connection points, a simpler approach is to draw parallel lines to the angle bisectors and intersect them with the spiral path to obtain the connection points. As shown in Figure 2g, through points $A_{0,2}$ and $B_{0,1}$, draw the parallel lines $L_{0,a}$ and $L_{0,b}$ of the line L (i.e., the angular bisector at vertex b_1) respectively. The points $A_{0,2}$ and $B_{0,1}$ are the endpoints of the articulated arcs and also points on the line $V_{2,3}b_1$ and line $b_1V_{1,1}$ at a distance $R_{min}/\tan(\frac{\theta_0}{2})$ from the point b_1 . The intersections of the straight lines $L_{0,a}$ and $L_{0,b}$ with the lines $V_{n+1,3}b_n$ and $b_nV_{n,1}$ are the endpoints of the subsequent articulated arcs. The articulated arcs at the other corners of the work area are generated in the same way. For angle θ_i (where $i = 1, 2, 3$), draw two parallel lines $L_{i,a}$ and $L_{i,b}$ to the angle bisectors through the two points on the sides of vertex $V_{1,i}$ at a distance of $R_{min}/\tan(\frac{\theta_i}{2})$. These parallel lines intersect the spiral path at points $A_{i,n}$ and $B_{i,n}$, where $i = 1, 2, 3$, which are the endpoints of the connecting arcs. The generation of the smooth spiral path is terminated when $R_{b_{n-1}V_{n-1,1}V_{n,2}V_{n,3}} \leq R_{min}$, ($R_{b_{n-1}V_{n-1,1}V_{n,2}V_{n,3}}$ is the radius of the smallest inscribed circle of quadrilateral $b_{n-1}V_{n-1,1}V_{n,2}V_{n,3}$). Consequently, a smooth spiral path is formed as shown in Figure 2g. At this point, the coverage path of the boundary area is generated, and the remaining blue area is the center region.

3.1.3 | Coverage Methods for the Center Region

The center region of the work area cannot be effectively covered using spiral paths, as doing so would result in significant overlap. Therefore, a separate path planning strategy is required for the central region. We developed two methods to achieve coverage path

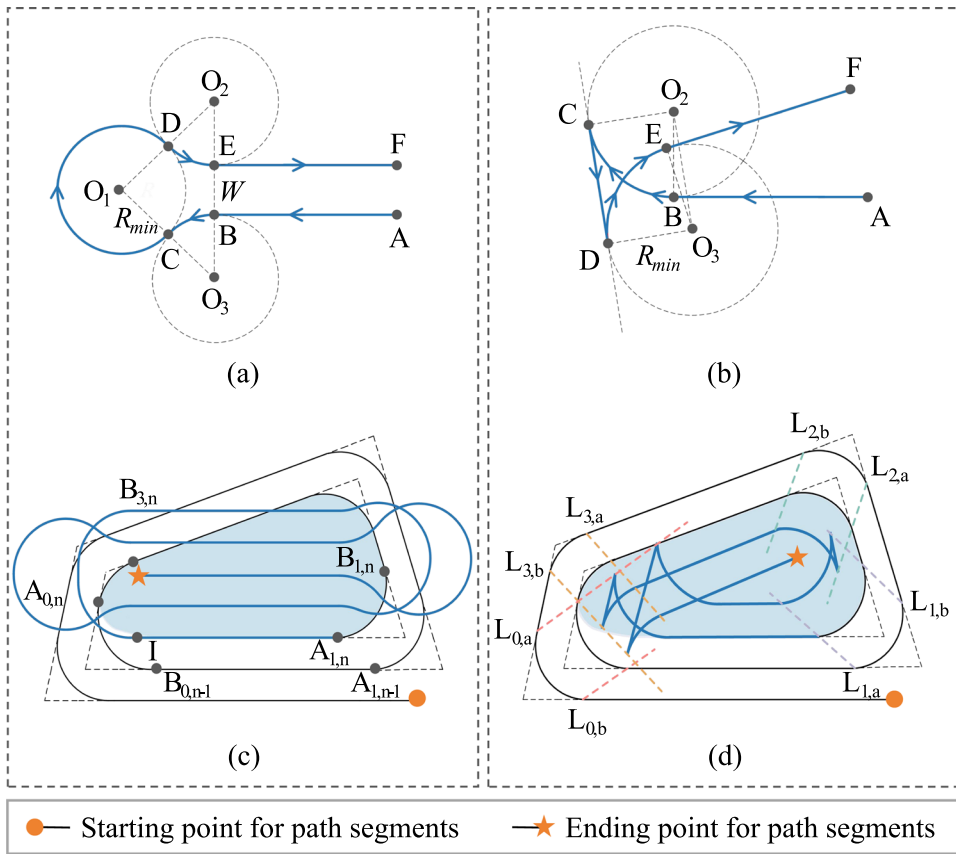


FIGURE 3 | Path steering approach in the center region. (a) and (b) show the schematic diagrams of the “Ω -shaped” steering path and “T-shaped” steering path, respectively; (c) and (d) show the complete paths in the center region for the two steering methods. [Color figure can be viewed at wileyonlinelibrary.com]

planning for the center region: the first method is the “Ω-shaped” steering coverage method with Dubins curves as connections, as shown in Figure 3a; and the second method is the “T-shaped” steering coverage, as shown in Figure 3b.

The “Ω-shaped” steering coverage method involves dividing the uncovered center region into parallel strips with a width of w . The parallel strips are parallel to the longest edge of the work area, as this reduces the number of strips as much as possible and thus reduces the number of times that the robot steers. The connection of these parallel strips is achieved through Dubins curves. In Figure 3a, points A, B, E and F are all known path points. AB and EF are strip paths that are parallel and equal in length to $IA_{l,n}$ in Figure 3c, point I is the intersection of edge $V_{n+1,0}V_{n+1,1}$ with edge $V_{n,0}V_{n,3}$. The connecting curve BCDE is composed of three tangent arcs with a radius of R_{min} . The length can be calculated using the equation

$$l_1 = R_{min} \left(3\pi - 4\sin^{-1} \left(\frac{2R_{min} + W}{4R_{min}} \right) \right), \quad (3)$$

where W is the distance between parallel strips. In Figure 3a, W represents the distance between paths AB and EF.

The “T-shaped” steering coverage method involves creating parallel paths in the center region along the longest edge and its opposite edge of the work area, and subsequently connecting these two paths

using a “T-shaped” path. The “T-shaped” path is shown in Figure 3b, it consists of two arcs and a line segment. Circle O_2 and circle O_3 are tangent to the contour-parallel path at point B and point E, respectively. The straight line CD is tangent to circle O_2 and circle O_3 at point C and point D, respectively. Suppose the robot enters the path from point A, travels along the path AB, follows the arc path BC to reach point C, reverses its direction along the path CD to point D, and then proceeds along the arc path DE to join the path EF. Where AB is the parallel path of the longest edge $V_{0,0}V_{0,1}$ of the work area; and EF is the parallel path of edge $V_{0,2}V_{0,3}$. Points A, B, E and F are known points, which are the intersection points of the articulated arcs with the edges $V_{n,0}V_{n,1}$ and $V_{n,2}V_{n,3}$, respectively. It can be noted that CD is parallel to $V_{n,0}V_{n,3}$. The lengths of the arc segments in the “T-shaped” steering path are equal to the lengths of the articulated arcs at the corresponding vertices, enabling the determination of the total length of the “T-shaped” steering path.

The paths generated by these two methods are illustrated in Figure 3c,d. Figure 3c shows the coverage path of the center region generated by the “Ω-shaped” steering coverage method, while Figure 3d shows the coverage path generated by the “T-shaped” steering coverage method. Both methods achieved coverage of the center region and only produced fewer overlapping.

For convex polygons, the paths are generated in the same way as for convex quadrilaterals, and the method is applicable to any convex polygonal region.

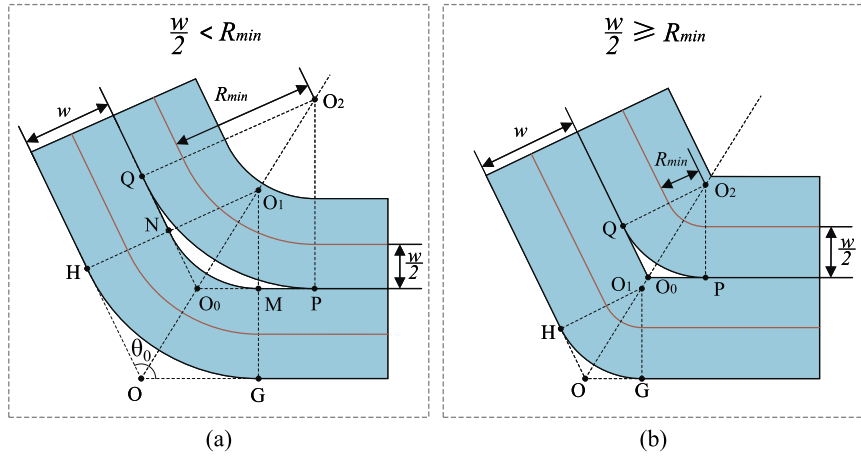


FIGURE 4 | Two cases of an outermost spiral path segment at the corner and its adjacent path segment. (a) the case of $\frac{w}{2} < R_{min}$; (b) the case of $\frac{w}{2} \geq R_{min}$. [Color figure can be viewed at wileyonlinelibrary.com]

3.2 | Evaluating Metric

Common evaluation metrics for CCPP algorithms include *TPL*, *ACR*, effective path ratio, and coverage time. In most headland pattern path planning research, the effective working area typically only considers the parallel strip region, excluding the headland region. This simplifies the calculation of the effective path length. However, when considering headland region, paths create overlapping coverage areas, which makes the calculation of effective path length more complex and challenging to express in an equation. Furthermore, these studies (Zhang et al. 2022; Mier, Valente, and de Bruin 2023; Nilsson and Zhou 2020b; Pour Arab, Spisser, and Essert 2023) often independently compare the *TPL* and *ACR* of CCPP algorithms, which can be unreasonable in some scenarios. To easily and effectively evaluate efficiency, it is crucial to consider both *ACR* and *TPL* in the comparison. Consequently, this study introduces a new evaluation metric: *PCE*, which is defined as follows:

$$\text{PathRatio} = \frac{\text{TPL}}{(\text{Coverage Area})/w}, \quad (4)$$

where $(\text{Coverage Area})/w$ represents the ideal shortest path length required to achieve coverage this area. When there is no overlapping, the value of $(\text{Coverage Area})/w$ is equal to the *TPL*, and Path ratio is equal to 1. When there is overlapping, the value of $(\text{Coverage Area})/w$ is less than the *TPL*, and path ratio is greater than 1. So path ratio is greater than or equal to 1.

$$\begin{aligned} \text{PCE} &= \frac{\text{ACR}}{\text{Path Ratio}} = \frac{(\text{Total Area}) \times \text{ACR}^2}{w \times \text{TPL}} \\ &= C \times \frac{\text{ACR}^2}{\text{TPL}}, \left(C = \frac{\text{Total Area}}{w} \right), \end{aligned} \quad (5)$$

where the value of *ACR* is in the range of [0–1]. When there is no overlapping coverage along the path, the *ACR* of the path equals the *PCE*. This implies that when all paths are effective, the higher the *ACR*, the higher the *PCE*. When the *ACR* reaches its maximum value of 1, the *PCE* also

reaches its maximum value of 1. However, when there is overlapping coverage along the path, the efficiency of the path is affected, and the *ACR* and *PCE* are no longer consistent. As a result, the value of *PCE* is less than 1 but greater than 0, indicating the presence of ineffective paths within the coverage. In other words, certain areas are covered multiple times. In such cases, with the coverage area remaining constant, a shorter *TPL* corresponds to higher coverage efficiency. A larger *PCE* value indicates a superior algorithm, which means that it can achieve greater area coverage with a shorter path, i.e., a more efficient coverage.

3.3 | Calculation of Area Coverage

Since robots moving along planned paths may result in overlapping coverage, and formalizing the area of these overlapping regions is complex, an alternative approach is to calculate the area of the uncovered regions. This method indirectly determines the area coverage ratio of the robot following the planned path. The paths generated by the spiral path planning method in convex polygons mainly have uncovered regions at the turns, and the uncovered area within the center region is negligible compared to the uncovered area at the turns. Therefore, the area of the uncovered regions is approximately equal to the sum of the areas uncovered at each turn. Figure 4a,b illustrates two cases of an outermost spiral path segment at the corner and its adjacent path segment, with the uncovered regions being OGH and QPMN or O₀PQ.

The area of OGH can be calculated using the following equation:

$$\begin{aligned} S_{OGH} &= S_{OGO_1H} - S_{O_1GH} = \frac{\left(R_{min} + \frac{w}{2}\right)^2}{\tan\left(\frac{\theta_0}{2}\right)} - \frac{180^\circ - \theta_0}{360^\circ} \pi \\ &\quad \left(R_{min} + \frac{w}{2}\right)^2. \end{aligned} \quad (6)$$

The area of region QPMN can be calculated by the following equation:

$$S_{QPMN} = S_{O_0PO_2Q} - S_{O_0MN} - S_{O_2PQ} = \frac{\left(R_{min} + \frac{w}{2}\right)^2}{\tan\left(\frac{\theta_0}{2}\right)} - \frac{\left(R_{min} - \frac{w}{2}\right)^2}{\tan\left(\frac{\theta_0}{2}\right)} + \frac{180^\circ - \theta_0}{360^\circ} \pi \left(R_{min} - \frac{w}{2}\right)^2 - \frac{180^\circ - \theta_0}{360^\circ} \pi \left(R_{min} + \frac{w}{2}\right)^2. \quad (7)$$

So the area of uncovered regions is

$$S_{uncovered-area} = (m - \pi) \left(R_{min} + \frac{w}{2} \right)^2 + (n - 1)(m - \pi) \left[\left(R_{min} + \frac{w}{2} \right)^2 - \left(R_{min} - \frac{w}{2} \right)^2 \right]. \quad (8)$$

Here, n represents the number of turns in the spiral path, and this value is related to w , R_{min} and the work area. m is a quantity related to the vertices of the work area, and its value is:

$$m = \frac{1}{\tan\left(\frac{\theta_0}{2}\right)} + \frac{1}{\tan\left(\frac{\theta_1}{2}\right)} + \dots + \frac{1}{\tan\left(\frac{\theta_{k-1}}{2}\right)}, \quad (9)$$

$$\left(\theta_i < 180^\circ, \sum_{i=0}^{k-1} \theta_i = (k-2) \cdot 180^\circ \right),$$

where k is the number of sides of the convex polygon. When $\frac{w}{2} \geq R_{min}$, the coverage of path is shown in Figure 4b, there is no overlap between regions O_0MN and the outer path segment, meaning the term $(n - 1)(m - \pi)(R_{min} - \frac{w}{2})^2$ equals zero. In this case, the equation can be simplified to:

$$S_{uncovered-area} = n \cdot (m - \pi) \left(R_{min} + \frac{w}{2} \right)^2, \quad (10)$$

when $\frac{w}{2} < R_{min}$, the coverage of path is shown in Figure 4a, there is an overlap between regions O_0MN and O_0MO_1N , meaning the term $(n - 1)(m - \pi)(R_{min} - \frac{w}{2})^2$ is not zero. In this case, the equation can be simplified to:

$$S_{uncovered-area} = (m - \pi) \left[\left(R_{min} + \frac{w}{2} \right)^2 + (n - 1) \cdot 2wR_{min} \right]. \quad (11)$$

Assuming the minimum inscribed circle radius of the work area is R , then $n = \lfloor (R - R_{min} + \frac{w}{2})/w \rfloor$, where symbol $\lfloor \cdot \rfloor$ denotes the floor function, $S_{uncovered-area}$ can be rewritten as:

$$S_{uncovered-area} = \begin{cases} \left(\frac{R - R_{min} + \frac{w}{2}}{w} \right) (m - \pi) \left(R_{min} + \frac{w}{2} \right)^2, & \left(\frac{w}{2} \geq R_{min} \right) \\ (m - \pi) \left[\left(R_{min} + \frac{w}{2} \right)^2 + \left(\left(\frac{R - R_{min} + \frac{w}{2}}{w} \right) - 1 \right) \cdot 2wR_{min} \right], & \left(\frac{w}{2} < R_{min} \right) \end{cases}. \quad (12)$$

Therefore, the area coverage ratio is given by:

$$S_{area_coverage} = 1 - \frac{S_{uncovered-area}}{S_{area}}, \quad (13)$$

S_{area} represents the area of the work region, and $S_{area_coverage}$ is the area coverage ratio. From Equations (9) and (12), it can be found that the area coverage ratio of the planned path is related to the parameters w and R_{min} . In other words, the area coverage ratio is influenced by the robot type and the width of the operating equipment. Therefore, with this area coverage calculation model of the spiral path, it is possible to solve for the optimal combination of parameters w and R_{min} that makes the coverage area maximized, which will be verified in the experimental part.

3.4 | High-Coverage-Rate Turning Strategy

When robots perform tasks, they are limited by battery capacity. Thus, maximizing coverage efficiency becomes critical. However, in scenarios requiring coverage of entire areas, such as patrolling or inspecting, ensuring absolute coverage of 100% takes precedence. In these situations, even if it means sacrificing efficiency, it's essential to ensure that every area is fully covered to meet mission requirements.

Notably, the spiral coverage path may leave some regions uncovered at the turns, as shown in Figure 5a. In response to this challenge, traditional approaches may try to reduce the offset distance between neighboring paths, but this often leads to overlap between paths, which in turn affects the coverage effect. So we propose a novel high-coverage-rate turning strategy, illustrated in Figure 5b and the decomposition diagram of the steering path with a high-coverage-rate turning strategy is shown in Figure 5c. The brown line represents the planned path, and the filled color indicates the area covered by the robot along the path. When the robot reaches a turn, it first follows the straight path S_1M_1 to point M_1 , then reverses from M_1 back to A_1 , follows the arc path A_1B_1 to B_1 , reverses along B_1N_1 to N_1 , and finally completes the turn by following the straight path N_1E_1 . By adopting this high-coverage-rate turning strategy, the uncovered regions at the turns of the spiral coverage path are significantly reduced and the overall area coverage of the path is increased.

4 | Experiments and Discussions

To evaluate the proposed coverage methods, we conducted five experiments: a *path coverage efficiency* metric characteristics analysis, a performance comparison, a coverage area calculation model validation, a high-coverage-rate turning strategy evaluation, and an airport runway field experiment. The characteristics of the *PCE* metric were analyzed through its functional relationship with *TPL* and *ARC*. The performance comparison experiment compared the proposed algorithms with the parallel coverage algorithm and deep reinforcement learning coverage algorithm to evaluate the performance in terms of *TPL*, *ACR*, and *PCE*. The accuracy of the proposed coverage area calculation model was verified by comparing the

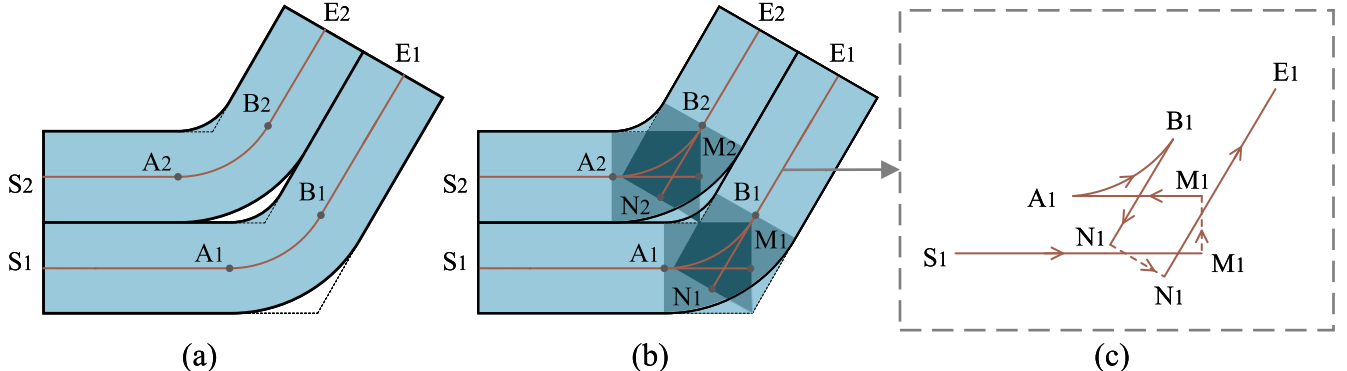


FIGURE 5 | (a) steering paths that do not employ a high-coverage-rate turning strategy. (b) steering path with high-coverage-rate turning strategy. (c) decomposition diagram of steering path with high-coverage-rate turning strategy. [Color figure can be viewed at [wileyonlinelibrary.com](#)]

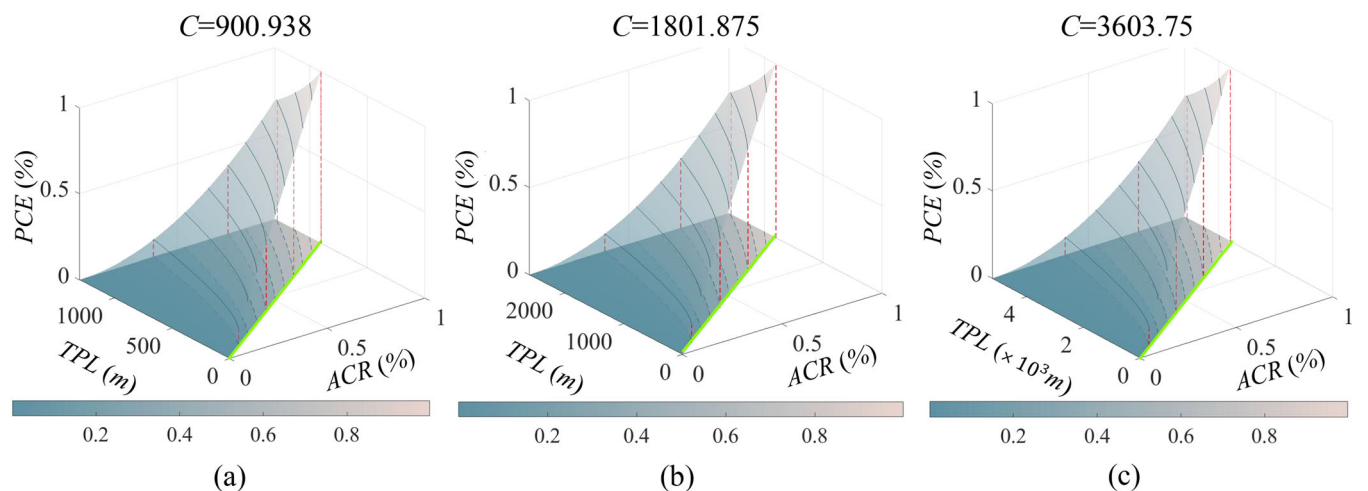


FIGURE 6 | The characteristics of PCE effected by parameters of ACR , TPL and C . (a), (b), (c) are the PCE function graphs when $C = 900.938$, 1801.875 , 3603.75 respectively. The solid lines on the surface are the contour lines, which take values from 0.1 to 0.9 in descending order; the red dashed lines are the projection lines; the green straight line is $TPL = C \times ACR$. ACR , area coverage ratio; PCE , path coverage efficiency; TPL , total path length. [Color figure can be viewed at [wileyonlinelibrary.com](#)]

coverage area calculated using the model with the coverage area obtained through pixel point statistics method. The high-coverage-rate turning strategy evaluation assessed by comparing the deviations in area coverage ratio of the paths obtained before and after implementing this strategy. In the airport runway field experiment, the effectiveness of the proposed method in real application scenarios was tested by using the method for planning inspection paths for robots in an actual airport runway region.

4.1 | Characteristic of Proposed Metric

This experiment shows the relationship between PCE , TPL , and ACR according to Equation (5). Assuming that the area of the region is 3603.75 m^2 and the coverage width is taken as 1, 2, and 3 m respectively, three sets of C values can be obtained. Then the three-dimensional function image of PCE with ACR and TPL is plotted, as shown in Figure 6.

Upon observing Figure 6a–c, it is evident that when ACR equals 1 and TPL equals C , PCE achieves its maximum value of 1. This indicates that when paths achieve complete coverage and the total length equals the ideal length required for full coverage, the PCE value reaches its maximum. Notably, this level of efficiency can only be attained in scenarios where robots can move omnidirectionally with a minimum turning radius of zero. Moreover, the relative distribution position of contour lines and the relative distribution pattern of the function graph remain consistent when C assumes different values. In addition, the contour lines on the graph of PCE function show a certain trend, increasing in the direction of ACR and decreasing with TPL . It is also noteworthy that the contours lines become denser around $TPL = C \times ACR$, which indicates that PCE is more sensitive to changes in ACR and TPL in this region. This sensitivity occurs because, at $TPL = C \times ACR$, all paths can be considered valid paths without overlap. Any additional path length added beyond this point, while ACR remains constant, is considered ineffective or redundant and affects the PCE .

TABLE 1 | Input convex quadrilateral, pentagonal, and octagonal regions.

Region name	Shape	Area/m ²	Vertex coordinates of the region/(m, m)
ISO-TRA		8123.74	(6.71,7), (27.21,89), (105.78,89), (126.28,7)
REC		11,988	(7,7), (7,81), (169,81), (169,7)
SQU		12,996	(7,7), (7,121), (121,121), (121,7)
PAR		8733	(2,3), (63.5,85), (170,85), (108.5,3)
IR-QUA		5154.624	(2.67,3), (19.18,60.78), (80.8,81.32), (93.17,3)
RA-TRA		3603.75	(3,3), (3,53), (64.66,53), (85.49,3)
Pentagon		19,700.88	(1.2935, 10.052), (9.5463, 15.1151), (19.107, 10.05653), (18.0894, 1), (2.3106, 1)
Octagon		2698	(0.37, 2.27332), (0.37, 4.275775), (1.7027, 5.9), (5.0473, 5.9), (6.38, 4.275775), (6.38, 2.27332), (5.046326, 0.7), (1.703674, 0.7)

Abbreviations: IR-QUA, irregular quadrilateral; ISO-TRA, isosceles trapezoid; PAR, parallelogram; RA-TRA, right-angle trapezoid; REC, rectangle; SQU, square.

Similarly, if *TPL* remains constant but *ACR* decreases slightly, indicating path overlap, the *PCE* will also be affected.

4.2 | Coverage Efficiency Performance of Our Spiral Path

We selected eight typical convex quadrilateral regions and other polygons to evaluate the coverage efficiency of our proposed spiral path planning method. The selected regions include an isosceles trapezoid (ISO-TRA), rectangle (REC), square (SQU), parallelogram (PAR), irregular quadrilateral (IR-QUA), right-angle trapezoid (RA-TRA), as well as pentagonal (Pentagon) and octagonal (Octagon) shapes, as shown in Table 1. This selection ensures that the evaluation reflects the adaptability and efficiency of our proposed methods in both regular and irregular environments. By focusing on these typical geometric configurations, we can demonstrate the generality and robustness of the algorithms across diverse types of regions. These shapes effectively represent different operational environments and complexities, allowing to thoroughly assess the performance of the methods. The robot's single coverage width was set to $w = 2$ m, and the minimum turning radius to $R_{min} = 4$ m. Then, the planning results of the two spiral coverage path planning methods proposed were compared with the traditional parallel coverage method (Bochtis and Vougioukas 2008) and the deep reinforcement learning coverage method (Jonnarth, Zhao, and Felsberg 2023) in these six regions. Since the deep reinforcement learning coverage method being compared is designed for unknown environments, whereas our method considers coverage in known environments, we ensured the fairness of the experiment by setting the sensor perception range parameter in the deep reinforcement learning method to be sufficiently large. In a polygonal region without obstacles, if the sensing range of the sensor is large enough, the environment can be considered as known.

In this set of experiments, we selected *TPL*, *ACR*, and *PCE* as the evaluation metrics for these methods. The *TPL* can be obtained directly during path generation. Calculating the *ACR* is more complex, especially when there are numerous overlapping coverage areas. To address this challenge, our method employs an imaging approach: initially, the generated path undergoes line width dilation to match the robot's coverage

width. Subsequently, the number of pixels corresponding to the path color in the image was counted. Finally, the path's *ACR* is calculated by dividing the pixel count by the total number of pixels occupied by the input area. Considering that the *ACR* of path generated by deep reinforcement learning method is preset as a termination condition for the method, we set the target *ACR* to be consistent with the *ACR* obtained by our method, and then compare the *TPL* and *PCE* with our methods. Figure 7 shows the path planning results of these methods in the ISO-TRA area. From the figure, it is evident that the parallel coverage method leaves several areas uncovered, while the deep reinforcement learning-based coverage method generates many overlaps. In contrast, the two spiral paths proposed in this paper effectively minimize both uncovered areas and overlaps. The experimental results are presented in Table 2. From the experimental results shown in Table 2, it can observe:

- 1 *TPL*: Upon examining the lengths of coverage paths in the eight selected areas, it is found that in ISO-TRA, REC, SQU, PAR, RA-TRA, and Octagon, the “T-shaped” spiral coverage path planning algorithm saves between 3.638%–8.816% in *TPL* compared to the parallel coverage method. While in ISO-TRA, REC, SQU, PAR, and RA-TRA, the “Ω-shaped” spiral coverage path planning algorithm saves between 2.098%–6.08% in *TPL* compared to the parallel coverage method. In the IR-QUA and Pentagon region, the “T-shaped” and “Ω-shaped” spiral coverage paths are 1.162%–3.675% and 5.067%–5.072% longer, respectively, than the parallel coverage method. Combining the experimental data from Table 2 with the path planning outcomes of the three algorithms in Pentagon and IR-QUA, as illustrated in Figure 8 and Figure 9d–f, it is observed that when the angle between the bottom edge (i.e., the edge parallel to the parallel strip path) and its nonadjacent edge is small, the parallel coverage path generates sparse paths in the headland area on the side of the nonadjacent edge. Consequently, the path length is shorter than the path length generated by the proposed method. However, this also results in a smaller *ACR*. Among the eight regions, the *TPL* of the path generated by the deep reinforcement learning method is the largest. The *TPL* of the “T-shaped” spiral coverage paths and “Ω-shaped” spiral coverage paths are 67.592%–78.319% and 66.62%–78.028% less than those of paths obtained by deep reinforcement learning method, respectively.

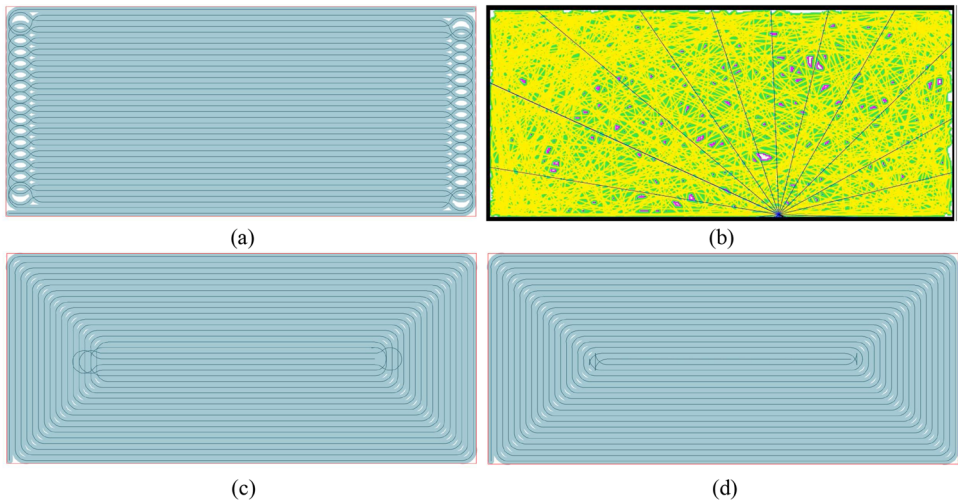


FIGURE 7 | (a) Parallel coverage path. (b) The coverage path obtained based on deep reinforcement learning (Jonnarth, Zhao, and Felsberg 2023), where the yellow line represents the path and the green area represents the already covered area. (c) Our proposed “Ω -shaped” spiral coverage path. (d) Our proposed “T-shaped” spiral coverage path. [Color figure can be viewed at [wileyonlinelibrary.com](#)]

TABLE 2 | The performance of four algorithms in different regions.

Region name	Evaluation metrics	Parallel coverage path (Bochtis and Vougioukas 2008)	Deep reinforcement learning coverage path (Jonnarth, Zhao, and Felsberg 2023)	“Ω-shaped” spiral coverage path (our)	“T-shaped” spiral coverage path (our)
ISO-TRA	TPL/m	4210.265	14739.714	4037.013	3926.216
	ACR/%	95.806	96.327	96.327	96.142
	PCE/%	88.553	25.570	93.360	95.626
REC	TPL/m	6154.486	24083.892	6025.394	5890.673
	ACR/%	97.494	98.005	98.005	97.979
	PCE/%	92.572	23.905	95.549	97.682
SQU	TPL/m	6746.626	25464.362	6423.232	6358.000
	ACR/%	96.412	97.162	97.162	97.137
	PCE/%	89.527	24.090	95.504	96.435
PAR	TPL/m	4393.114	12928.305	4210.054	4105.364
	ACR/%	95.586	93.696	93.696	93.268
	PCE/%	90.812	29.651	91.051	92.522
IR-QUA	TPL/m	2452.562	7859.513	2576.951	2481.058
	ACR/%	86.595	95.112	95.112	94.791
	PCE/%	78.807	29.665	90.476	93.339
RA-TRA	TPL/m	1891.268	5321.362	1776.286	1724.543
	ACR/%	94.258	94.655	94.655	94.596
	PCE/%	84.646	30.338	90.886	93.497
Pentagon	TPL/m	9659.412	46190.09	10148.878	10014.38
	ACR/%	93.45	98.927	98.927	98.83
	PCE/%	95.3	20.871	96.018	97.21
Octagon	TPL/m	1412.518	5981.283	1428.782	1361.131
	ACR/%	91.768	99.414	99.414	99.245
	PCE/%	87.641	22.29	93.863	98.36

Abbreviations: ACR, area coverage ratio; IR-QUA, irregular quadrilateral; ISO-TRA, isosceles trapezoid; PAR, parallelogram; PCE, path coverage efficiency; RA-TRA, right-angle trapezoid; REC, rectangle; SQU, square; TPL, total path length.

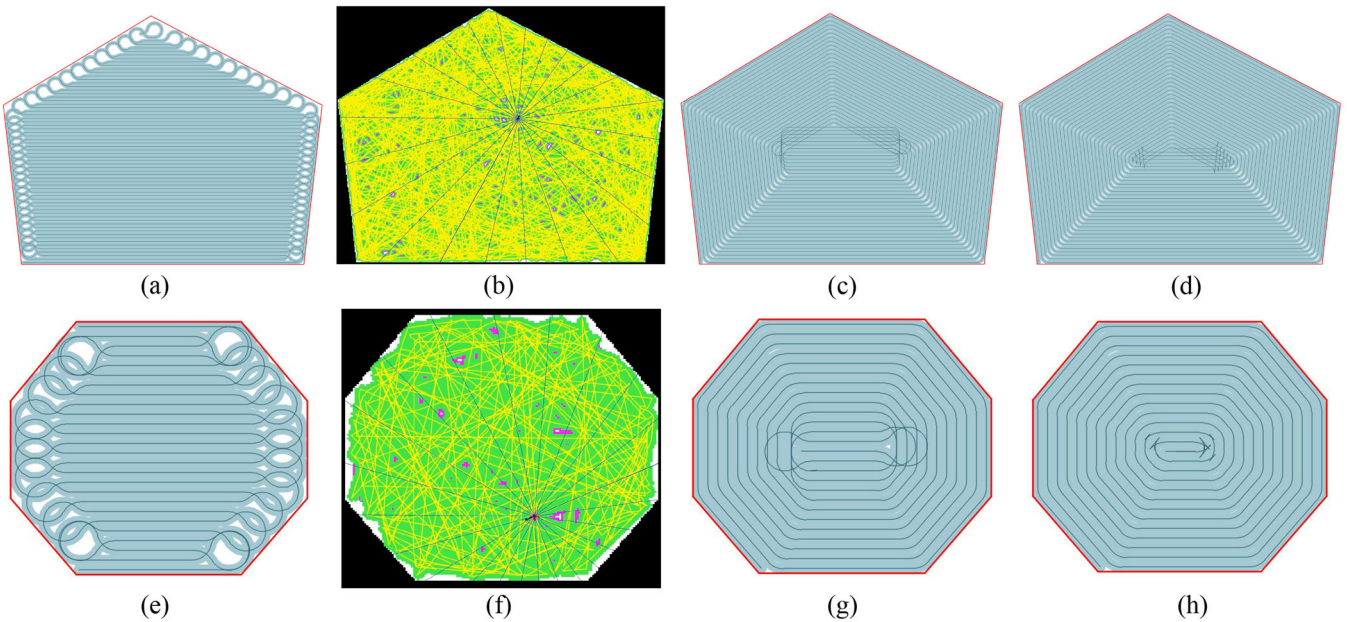


FIGURE 8 | Path planning results in the pentagon and octagon. (a) (e) Parallel coverage path. (b) (f) The coverage path obtained based on deep reinforcement learning (Jonnarth, Zhao, and Felsberg 2023), where the yellow line represents the path and the green area represents the already covered area. (c) (g) Our proposed “Ω -shaped” spiral coverage path. (d) (h) Our proposed “T-shaped” spiral coverage path. [Color figure can be viewed at [wileyonlinelibrary.com](#)]

2 *ACR*: Upon observing the *ACR* of the three algorithms in the six selected regions, it is found that the “T-shaped” spiral coverage path and the “Ω-shaped” spiral coverage path are very similar in terms of *ACR*. In the input regions ISO-TRA, REC, SQU, IR-QUA, RA-TRA, Pentagon, and Octagon, the *ACR* of the paths generated by the proposed method are higher than those of the paths generated by the parallel coverage method. The *ACR* of the “T-shaped” and “Ω-shaped” spiral coverage paths exceed that of the parallel coverage paths by 0.335%–8.196% and 0.397%–8.518% respectively. However, in the PAR region, their *ACR* is lower than the parallel coverage path by 2.318% and 1.89% respectively. Combining the experimental data from Table 2 and the path planning results of the three algorithms in PAR are shown in Figure 9a–c, it is observed that when a region has a small vertex angle, the proposed methods result in more uncovered areas at the turn near that vertex. Therefore, the coverage area may be smaller than that of the parallel coverage method, but the paths generated by the proposed methods are shorter.

3 *PCE*: The “T-shaped” spiral coverage path planning algorithm shows a path coverage efficiency that is 0.930%–4.497% higher than the “Ω-shaped” algorithm. Comparatively, the path coverage efficiency of the parallel coverage method is lower by 1.709%–14.538% and 0.238%–11.676% than the two proposed spiral coverage algorithms, the *PCE* of the deep reinforcement learning method is 62.871%–76.339% and 60.548%–75.147% lower than the two proposed spiral coverage algorithms, respectively. Consequently, the “T-shaped” algorithm has the best performance in terms of path coverage efficiency.

Figure 9

The experimental results demonstrate that compared to the parallel coverage method, the “T-shaped” and “Ω-shaped”

spiral coverage path planning algorithms not only reduce the total path length but also maintain a higher area coverage ratio in most regions. This advantage stems from the fact that spiral paths are generated progressively from the outside in, allowing the robot to move continuously without frequent turning maneuvers, which are common in the parallel coverage method, especially in the headland area. These turns often lead to path overlap and missed coverage. Moreover, the “T-shaped” algorithm exhibited superior performance in terms of path coverage efficiency, consistently outperforming other methods, including the deep reinforcement learning-based approach, which resulted in the longest paths and the lowest efficiency. Spiral paths adapt to the shape of the region, generating an inward-moving coverage path that effectively minimizes overlap. In contrast, the deep reinforcement learning method requires continuous interaction with the environment to explore the coverage path, leading to more redundant paths and lower efficiency. Although the spiral path algorithm faces some challenges in regions with narrow vertex angles, the proposed methods are overall more efficient in complex multi-vertex regions. These findings validate the effectiveness and adaptability of the proposed algorithms across various shapes, highlighting their potential in practical applications that require optimized path efficiency and complete coverage.

4.3 | Coverage Area Calculation Model

In practical scenarios, the choice of R_{min} and w values is related to how robots or operating equipment are selected. To explore the optimal combination of input parameters R_{min} and w that maximizes the area coverage ratio, and to validate the effectiveness of the proposed area model, the following experiment was conducted: The same six areas selected in performance comparison experiment were used as the experimental regions.

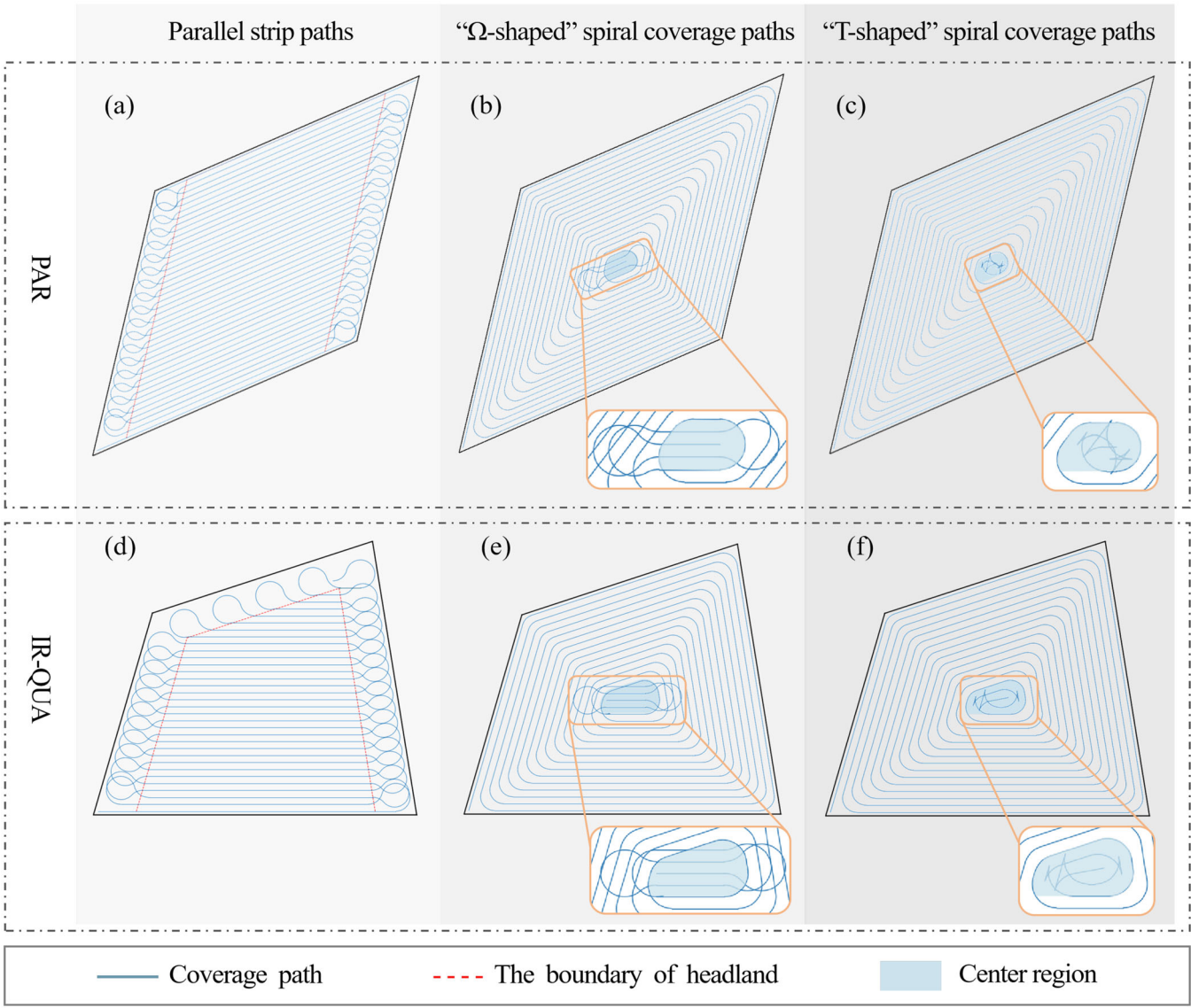


FIGURE 9 | Path planning results of three algorithms in PAR region and IR-QUA region. (a) Depicts the result of the parallel coverage path planning algorithm in the PAR region; (b) shows the result of the “Ω-shaped” spiral coverage path planning algorithm in the PAR region; (c) represents the result of the “T-shaped” spiral coverage path planning algorithm in the PAR region; (d) illustrates the result of the parallel coverage path planning algorithm in the IR-QUA region; (e) shows the result of the “Ω -shaped” spiral coverage path planning algorithm in the IR-QUA region; (f) depicts the result of the “T-shaped” spiral coverage path planning algorithm in the IR-QUA region. IR-QUA, irregular quadrilateral; PAR, parallelogram. [Color figure can be viewed at [wileyonlinelibrary.com](#)]

Since the coverage area calculation model proposed in Section 3.3 is segmented, two sets of w and R_{min} parameters were chosen. One set uses the parameters from Section 4.2: $w = 2$ m and $R_{min} = 4$ m, for the case where $\frac{w}{2} < R_{min}$. The other set is chosen as $w = 3$ m and $R_{min} = 1$ m, for the case where $\frac{w}{2} \geq R_{min}$.

According to the experimental results in Table 3, the mean error of the results obtained by the two methods is 0.000657, with a variance of $1.83e-7$. Therefore, the coverage area calculation model proposed in Section 3.3 is effective. Then, this model can be used to study the relationship between parameters R_{min} and w with the area coverage ratio. Here, region REC is selected as an example to show how to solve the optimal parameters R_{min} and w to maximize the coverage area through this model. The range of the robot's minimum turning radius is set between 2 m and 6 m, and the coverage width is set between 2 m and 12 m.

A nonlinear optimization problem is established to find the optimal combination of parameters (R_{min}, w) to maximize the area coverage ratio:

$$\begin{array}{ll} \min_{w, R_{min}} & 1 - S_{\text{area_coverage}} \\ \text{s.t.} & 2 < R_{min} < 6 \\ & 2 < w < 12 \\ & 0 \leq 1 - S_{\text{area_coverage}} \leq 1 \end{array}$$

The optimization objective function aims to minimize the uncovered area ratio of the path, with constraints on the optimization parameters R_{min} and w , as well as boundary constraints for the objective function. Since the objective function is a piecewise function and contains terms that involve floor functions, it is non-continuously

TABLE 3 | Results of ACR obtained by pixel point counting and the coverage area calculation model.

Two cases for the values of R_{min}, w	ACR calculation method	ISO-TRA	REC	SQU	PAR	IR-QUA	RA-TRA
$\frac{w}{2} < R_{min}$	Pixel point counting/% (baseline)	96.1417	97.9787	97.1375	93.2676	94.7909	94.5963
	Coverage area calculation model/%	96.2183	97.9879	97.1928	93.3392	94.8682	94.7377
$\frac{w}{2} \geq R_{min}$	Pixel point counting/% (baseline)	98.9537	99.4703	99.2509	98.1993	98.5714	98.5409
	Coverage area calculation model/%	99.0183	99.5077	99.2569	98.2710	98.7119	98.5778

Abbreviations: ACR, area coverage ratio; IR-QUA, irregular quadrilateral; ISO-TRA, isosceles trapezoid; PAR, parallelogram; RA-TRA, right-angle trapezoid; REC, rectangle; SQU, square.

differentiable, making this nonlinear problem challenging to solve analytically. Numerical optimization methods are required to find a solution. Additionally, the objective function likely has multiple extremal points. To avoid converging to local minima, we choose a global optimization algorithm—the Genetic Algorithm—to solve this optimization problem. The application of the coverage area calculation model in other regions is consistent with the application in region REC.

From the iteration results of the genetic algorithm in Figure 10, after 78 iterations, the objective function converges to 0.9415%. The optimal parameter combination achieving this minimum value is $(R_{min}, w) = (2.0004, 4.6671)$. With $R_{min} = 2.0004\text{m}$ and $w = 4.6671\text{m}$, the area coverage ratio calculated using the pixel point counting method is 98.86151%, and the error compared to the solution obtained by the genetic algorithm is 0.19699%. Therefore, when selecting parameters, the coverage area calculation model obtained in Section 3.3 can be used, and the genetic algorithm can be employed to optimize and find the optimal combination of robot parameters. The optimal combination of R_{min} and w can serve as a reference for the selection of the robot and the operating equipment.

4.4 | High-Coverage-Rate Turning Strategy

When R_{min} and w are fixed, and the goal is to achieve near-complete area coverage, a high-coverage-rate turning strategy can be used to enhance the area coverage ratio of spiral path. For this approach, we select the same six typical convex quadrilateral areas for CCPP. The single coverage width of the robot is still set at $w = 2\text{ m}$, and the minimum turning radius is $R_{min} = 4\text{m}$. The results obtained are presented in Table 4:

The experimental results show that the spiral coverage paths obtained using the high-coverage-rate turning strategy achieved an area coverage ratio of 100% in the selected six areas, realizing complete coverage. Moreover, the coverage significantly improved compared to the paths that do not utilize the high-coverage-rate turning strategy, with an increase ranging from 2.021% to 6.732%. However, this also resulted in a certain trade-off, sacrificing 14.1434% to 23.5197% of coverage efficiency.

To justify the utility of our proposed turning strategy despite the efficiency trade-off, we compared and analyzed it with the parallel stripe coverage method proposed in the literature (Jeon

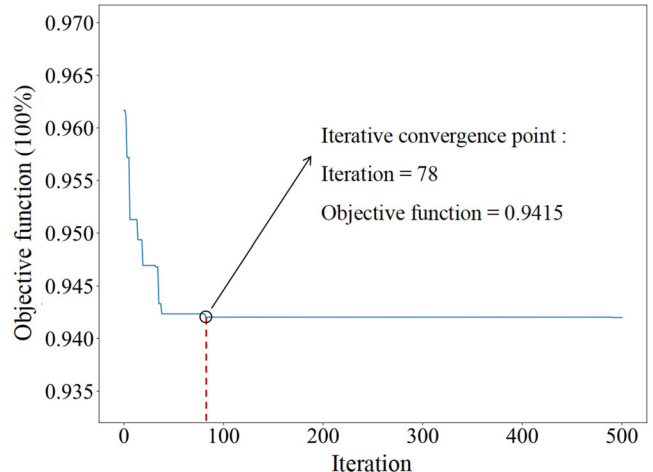


FIGURE 10 | Iteration curve for solving the minimum uncovered area ratio using genetic algorithm. [Color figure can be viewed at wileyonlinelibrary.com]

et al. 2021), and the deep reinforcement learning method proposed in the literature (Jonnarth, Zhao, and Felsberg 2023), both of which prioritize achieving 100% coverage. The test area selected for comparison aligns with the parameters described in (Jeon et al. 2021), with an area of 3467.74 m^2 and robot coverage width of 2.4 m . The experimental results are presented in Table 5 and Figure 11.

Figure 11 shows that the parallel coverage method from the literature (Jeon et al. 2021) results in significant overlap in the headland areas on both sides, and the deep reinforcement learning-based coverage method generates even more overlap. In contrast, our proposed method exhibits only slight overlap at the turns. From the experimental results in Table 5, it can be seen that our spiral coverage method using a high-coverage-rate turning strategy achieved 100% coverage, which is 0.62% higher than the parallel coverage method in literature (Jeon et al. 2021) and 0.6% higher than the deep reinforcement learning method (Jonnarth, Zhao, and Felsberg 2023). In addition, our method saves 318.5 m of path length compared to the parallel coverage method, and the path coverage efficiency is 18.5% higher. Compared with deep reinforcement learning-based method, our approach saves 4708.426 m of path length and achieves a 49.13% increase in path coverage efficiency. Although our method sacrifices some coverage efficiency to achieve complete coverage, its path coverage efficiency is still higher than existing methods.

TABLE 4 | ACR of the algorithm before and after adopting the high-coverage-rate turning strategy.

Base method	Using strategy	Evaluation metrics	Region name					
			ISO-TRA	REC	SQU	PAR	IR-QUA	RA-TRA
Spiral coverage path	X	ACR/%	96.142	97.979	97.137	93.268	94.791	94.596
		TPL/m	3926.216	5890.673	6358.000	4105.364	2481.058	1724.543
		PCE/%	95.626	97.683	96.434	92.522	93.339	93.497
	√	ACR/%	100	100	100	100	100	100
		TPL/m	5315.426	7175.063	8224.901	5799.074	3642.043	2574.955
		PCE/%	76.417	83.539	79.004	75.297	70.766	69.977
Deviations in area coverage ratio			3.858	2.021	2.863	6.732	5.209	5.404

Abbreviations: *ACR*, area coverage ratio; *IR-QUA*, irregular quadrilateral; *ISO-TRA*, isosceles trapezoid; *PAR*, parallelogram; *PCE*, path coverage efficiency; *RA-TRA*, right-angle trapezoid; *REC*, rectangle; *SQU*, square; *TPL*, total path length.

TABLE 5 | Results of parallel coverage paths and spiral coverage paths using the high-coverage-rate turning strategy in the testing area.

Method	ACR/%	TPL/m	PCE/%
Parallel path (Jeon et al. 2021)	99.38	2831.4	50.4
Deep reinforcement learning coverage path (Jonnarth, Zhao, and Felsberg 2023)	99.4	7221.326	19.77
Spiral path (our)	100	2512.9	68.9

Abbreviations: *ACR*, area coverage ratio; *PCE*, path coverage efficiency; *TPL*, total path length.

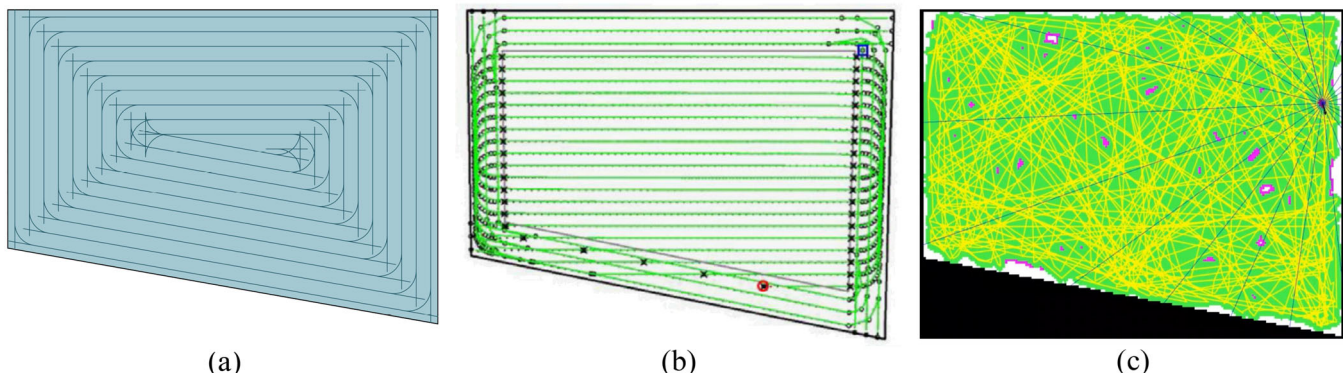


FIGURE 11 | (a) The path planning results obtained by combining our spiral coverage algorithm with our proposed high-coverage-rate turning strategy. (b) The parallel coverage method in literature (Jeon et al. 2021). (c) The coverage path obtained based on deep reinforcement learning (Jonnarth, Zhao, and Felsberg 2023). [Color figure can be viewed at [wileyonlinelibrary.com](#)]

4.5 | Airport Runway Field Experiment

An airport runway refers to an elongated area within an airport designated for the takeoff or landing of aircraft. The intrusion of foreign objects onto airport runways not only severely impacts normal flight operations but also increases the possibility of aviation accidents. Therefore, runway inspection at the airport is indispensable. In the context of the robot's runway inspection task at the airport, we conducted an actual site coverage path planning experiment on the north runway of Beijing Daxing Airport for robot inspection tasks on the airport runway. The design and process of the entire experiment are shown in Figure 12.

Due to the full length of the runway being approximately 3.6 km, we selected a segment for testing. The latitude and

longitude of the four vertices in the selected area were obtained through Real Time Kinematic (RTK) positioning technique with centimeter-level accuracy. First, the RTK base station should be set up outside the test area and in an open area. Then, the RTK mobile station should be placed at the vertex positions of the test area for measurement, and the results are presented in Table 6 and Figure 13.

The position data acquired by the RTK device is initially in the WGS-84 (World Geodetic System 1984) coordinate system. For the convenience of subsequent path planning tasks, it is necessary to convert the collected latitude and longitude coordinate data to a coordinate system in meters. First, the position data is converted from the WGS-84 coordinate system to the UTM (Universal Transverse Mercator, a universal transverse

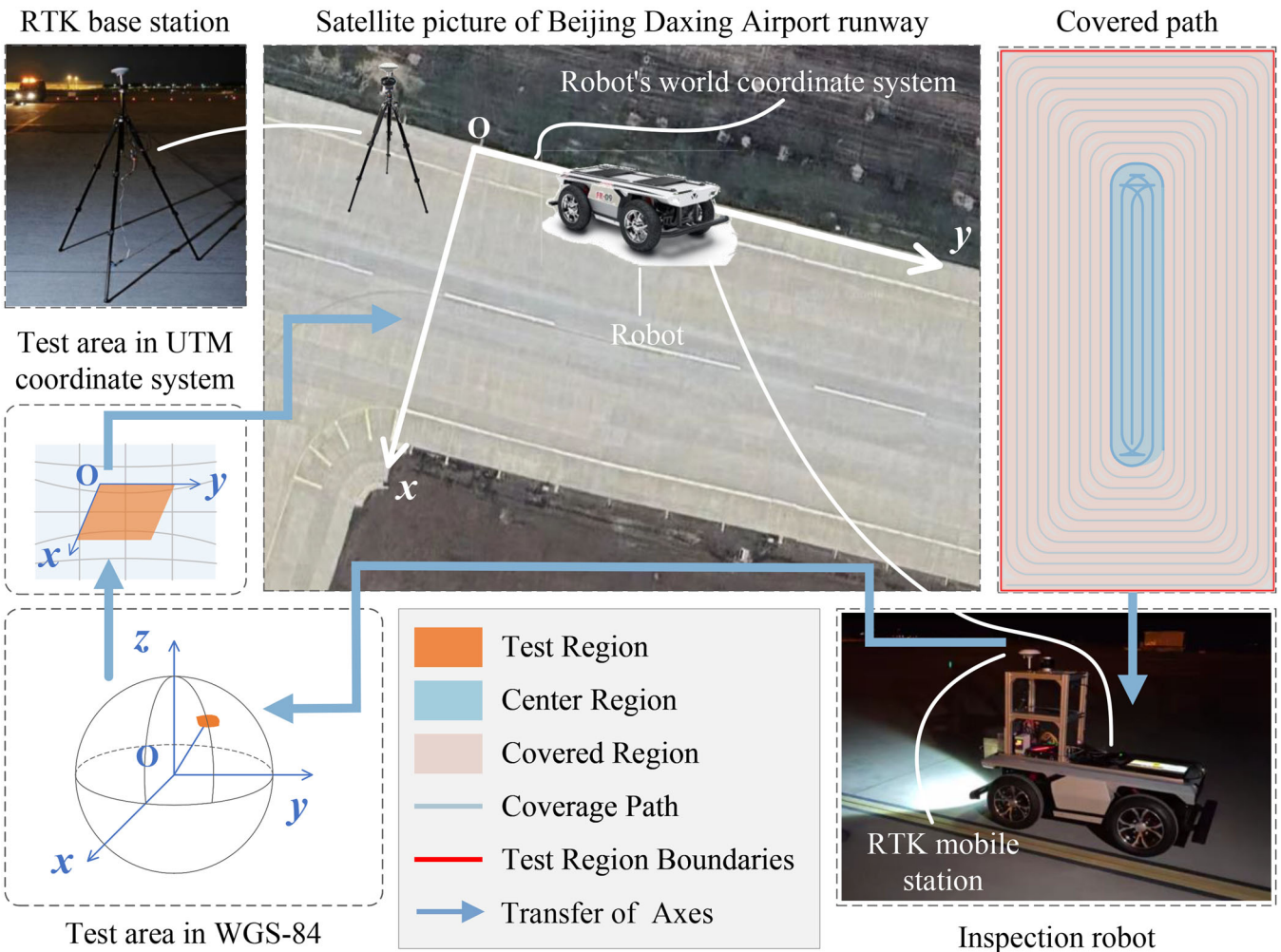


FIGURE 12 | The design and process of the airport runway field experiment. [Color figure can be viewed at [wileyonlinelibrary.com](#)]

TABLE 6 | Table of points with latitude and longitude.

Point name	Latitude (°)	Longitude (°)
P ₁	39.51722	116.44372
P ₂	39.51654	116.44355
P ₃	39.51452	116.45468
P ₄	39.51517	116.45490

Mercator projection) coordinate system to achieve the transition from geographical coordinates to meters. Next, a dedicated robot coordinate system is established with P₁ as the origin, P₂ as a point on the x-axis, and P₄ as a point on the y-axis. Through translation and rotation, the UTM coordinate system can be converted to the self-defined robot coordinate system. Given the large values of position coordinates in the UTM coordinate system, converting them to the self-defined robot coordinate system simplifies robot localization.

After the conversion, it is known that the area of the selected region is approximately 43200 m², with the length and width measuring 720 m and 60 m, respectively. The size of the inspection robot is 1600 × 820 × 1150 mm. The inspection robot utilizes the Ackermann steering structure with a minimum turning radius of $R_{min} = 2.1$ m. The pavement detection sensor it is equipped with has an inspection range of 1 m wide, denoted as $w = 2$ m. The robot's speed is 6 m/s. With the test region and robot data available, these inputs can be used in the path generator for path planning. Then, the planned paths are given to the robot to execute. The robot's path tracking employs a phased control strategy: the PID controller is used for straight-line path tracking, while a geometry-based control method is applied for turning paths, where control parameters are derived from the path curvature and the robot's motion model. By combining the strengths of both methods for



FIGURE 13 | The airport runway test area. [Color figure can be viewed at [wileyonlinelibrary.com](#)]

TABLE 7 | Results of airport runway field experiment.

Method	TPL/m	ACR/%	PCE/%	Execution time/s
Parallel strip path	1892.63	96.296	91.424	3662
“Ω-shaped” spiral coverage path (our)	1877.64	99.190	97.777	3614
“T-shaped” spiral coverage path (our)	1858.80	99.201	98.790	3610

Note: The TPL data and ACR data were obtained after ignoring the paths in the middle portion of the test region because the three methods formed the same paths in the middle region. The length of the middle region is 657.8 m.

Abbreviations: ACR, area coverage ratio; PCE, path coverage efficiency; TPL, total path length.

different path types, the overall tracking errors during the process are reduced.

The proposed methods and the parallel coverage method are used to plan the paths for the test region, respectively. The performance of the paths obtained by the three methods in the various metrics is shown in Table 7.

From the experimental results, it can be seen that the “T-shaped” spiral coverage path and “Ω-shaped” spiral coverage path saves 1.79% and 0.792% of the path length than the parallel coverage path respectively in total path length. The “T-shaped” spiral coverage path and the “Ω-shaped” spiral coverage path cover 2.894% and 2.905% more area than the parallel coverage path, respectively. In path coverage efficiency, the “T-shaped” spiral coverage path and the “Ω-shaped” spiral coverage path are 7.366% and 6.353% higher than the parallel coverage path, respectively. Due to the complexity of Dubins curves, the robot will take more time to execute Dubins curve steering than simple circular steering curves. The “T-shaped” spiral coverage path and the “Ω-shaped” spiral coverage path save 1.42% and 1.31% of time, respectively, compared to parallel coverage path. In summary, the proposed methods outperform the traditional parallel coverage method in all four metrics compared.

5 | Conclusion

In this study, we address the challenges faced by nonomnidirectional robots in realizing full-coverage operations, in particular, their limited turning capacity and the overlap path coverage issue prevalent in existing algorithms. Our contribution is the development of a new partitioned coverage method for nonomnidirectional robots by designing spiral coverage path at the boundary region that adhere to the robot's kinematics and two coverage methods with low overlap rates for the remaining center region. The method effectively reduces the complexity of the coverage task and provides a solution to improve the path coverage efficiency and optimize the path planning strategy. Then, we introduce a new path coverage efficiency metric that addresses the issue of comprehensively evaluating the performance of coverage algorithm. This metric provides a more comprehensive understanding of the coverage efficiency and is characterized by simplicity of calculation and wide applicability. Experimental results show that our spiral coverage path planning algorithm is superior to traditional parallel coverage methods and CCPP method based on deep reinforcement learning. Specifically, our algorithm achieves 0.238%–14.538% higher path coverage efficiency than traditional method, 60.548%–76.339% higher than deep reinforcement

learning-based methods, and reduces overlapping, which is a significant progress in application scenarios where energy consumption is a limiting factor. According to the experimental results, it can be found that although learning based methods have advantages in full coverage path planning tasks in unknown environments, traditional methods are more suitable in known environments. In addition, we develop an effective area coverage calculation model that provides valuable insights for selecting appropriate robots and operating equipment in real-world applications. Furthermore, we introduce a high-coverage-rate turning strategy designed for spiral paths. This strategy fulfills the urgent need for full coverage for tasks such as patrolling and exploration. Compared to spiral paths without this turn strategy, the paths with this strategy significantly improved area coverage by 2.021%–6.732%, achieving 100% area coverage. Finally, our field experiment conducted on an airport runway validated the practicality and efficiency of our proposed method. The results indicated a time-saving of 1.42% compared to traditional method, underscoring the effectiveness and potential real-world applicability of our approach.

In summary, our research not only contributes to advancing the field of CCPP for nonomnidirectional robots but also offers practical solutions to enhance efficiency and effectiveness in various application scenarios. Our method is highly adaptable and can be applied to various scenarios, including service robots for cleaning tasks, robots in smart manufacturing for inspection and maintenance, and medical robots for disinfection purposes. The ability to ensure complete coverage while optimizing path efficiency makes our method valuable for these applications. Future work will focus on further testing and refining our method in more complex environments, including those with obstacles and dynamic elements, to broaden its applicability and robustness. While our method has proven effective in static environments, future research will refine our method to handle dynamic environments with moving obstacles. This involves developing adaptive algorithms that can respond in real-time to environmental changes, ensuring continuous coverage and optimal path planning. In addition, exploring the integration of our path planning method with multi-robots systems can significantly improve coverage efficiency and reduce overall task completion time. Coordinating multiple robots to work together is a promising direction for future work.

Acknowledgments

Young Elite Scientists Sponsorship Program by CAST (Grant No. 2022QNRC001), the National Natural Science Foundation of China (Grant No. 62103035), and the Beijing Natural Science Foundation (Grant Nos. 3222016 and L231004).

Data Availability Statement

The data that support the findings of this study are available from the corresponding author upon reasonable request.

References

- Bakhtiari, A. A., H. Navid, J. Mehri, and D. D. Bochtis. 2011. "Optimal Route Planning of Agricultural Field Operations Using Ant Colony Optimization." *Agricultural Engineering International: CIGR Journal* 13, no. 4: 1–10.
- Bochtis, D., C. Sørensen, and S. Vougioukas. 2010. "Path Planning for In-Field Navigation-Aiding of Service Units." *Computers and Electronics in Agriculture* 74, no. 1: 80–90. <https://doi.org/10.1016/j.compag.2010.06.008>.
- Bochtis, D., and S. Vougioukas. 2008. "Minimising the Non-Working Distance Travelled By Machines Operating in a Headland Field Pattern." *Biosystems Engineering* 101, no. 1: 1–12. <https://doi.org/10.1016/j.biosystemsg.2008.06.008>.
- Bochtis, D., S. Vougioukas, and H. Griepentrog. 2009. "A Mission Planner for an Autonomous Tractor." *Transactions of the ASABE* 52, no. 5: 1429–1440. <https://doi.org/10.13031/2013.29123>.
- Bormann, R., F. Jordan, W. Li, J. Hampp, and M. Hägele. 2016. "Room Segmentation: Survey, Implementation, and Analysis." In *2016 IEEE International Conference on Robotics and Automation (ICRA)*, 1019–1026. Stockholm, Sweden: IEEE.
- Bosse, M., N. Nourani-Vatani, and J. Roberts. 2007. "Coverage Algorithms for an Under-Actuated Car-Like Vehicle in an Uncertain Environment." In *Proceedings 2007 IEEE International Conference on Robotics and Automation*, 698–703. Rome, Italy: IEEE.
- Cabreira, T. M., C. Di Franco, P. R. Ferreira, and G. C. Buttazzo. 2018. "Energy-Aware Spiral Coverage Path Planning for UAV Photogrammetric Applications." *IEEE Robotics and Automation Letters* 3, no. 4: 3662–3668.
- Cao, Y., Y. Han, J. Chen, X. Liu, Z. Zhang, and K. Zhang. 2019. "Optimal Coverage Path Planning Algorithm of the Tractor-Formation Based on Probabilistic Roadmaps." In *2019 IEEE International Conference on Unmanned Systems and Artificial Intelligence (ICUSA)*, 27–32. Xi'an, China: IEEE.
- Carvalho, J. P., and A. P. Aguiar. 2023. "A Reinforcement Learning Based Online Coverage Path Planning Algorithm." In *2023 IEEE International Conference on Autonomous Robot Systems and Competitions (ICARSC)*, 81–86. Tomar, Portugal: IEEE.
- Choi, Y.-H., T.-K. Lee, S.-H. Baek, and S.-Y. Oh. 2009. "Online Complete Coverage Path Planning for Mobile Robots Based on Linked Spiral Paths Using Constrained Inverse Distance Transform." In *2009 IEEE/RSJ International Conference on Intelligent Robots and Systems*, 5788–5793. IEEE.
- Conesa-Muñoz, J., G. Pajares, and A. Ribeiro. 2016. "Mix-Opt: A New Route Operator for Optimal Coverage Path Planning for a Fleet in an Agricultural Environment." *Expert Systems With Applications* 54, no. 1: 364–378. <https://doi.org/10.1016/j.eswa.2015.12.047>.
- De Berg, M. 2000. *Computational Geometry: Algorithms and Applications*. Cham: Springer Science & Business Media.
- Edwards, G. T., J. Hinge, N. Skou-Nielsen, A. Villa-Henriksen, C. A. G. Sørensen, and O. Green. 2017. "Route Planning Evaluation of a Prototype Optimised Infield Route Planner for Neutral Material Flow Agricultural Operations." *Biosystems Engineering* 153, no. 4: 149–157. <https://doi.org/10.1016/j.biosystemsg.2016.10.007>.
- Engelsons, D., M. Tiger, and F. Heintz. 2022. "Coverage Path Planning in Large-scale Multi-Floor Urban Environments With Applications to Autonomous Road Sweeping." In *2022 International Conference on Robotics and Automation (ICRA)*, 3328–3334. Philadelphia, PA, USA: IEEE.
- Evans, J. T., S. K. Pitla, J. D. Luck, and M. Kocher. 2020. "Row Crop Grain Harvester Path Optimization in Headland Patterns." *Computers and Electronics in Agriculture* 171, no. 212: 105295. <https://doi.org/10.1016/j.compag.2020.105295>.
- Gabriely, Y., and E. Rimon. 2002. "Spiral-stc: An on-line Coverage Algorithm of Grid Environments by a Mobile Robot." In *Proceedings 2002 IEEE International Conference on Robotics and Automation (Cat. No. 02CH37292)*, 954–960. Washington, DC, USA: IEEE.
- Gonzalez, E., M. Alarcon, P. Aristizabal, and C. Parra. 2003. "BSA: A Coverage Algorithm." In *Proceedings 2003 IEEE/RSJ International Conference on Intelligent Robots and Systems (IROS 2003)(Cat. No. 03CH37453)*, 1679–1684. Las Vegas, NV: IEEE.
- Grissom, R. D., M. F. Kocher, V. I. Adamchuk, P. J. Jasa, and M. A. Schroeder. 2004. "Field Efficiency Determination Using Traffic Pattern Indices." *Applied Engineering in Agriculture* 20, no. 5: 563–572. <https://doi.org/10.13031/2013.17456>.
- Hameed, I. A. 2017. "Coverage Path Planning Software for Autonomous Robotic Lawn Mower Using Dubins' Curve." In *2017 IEEE International Conference on Real-time Computing and Robotics (RCAR)*, 517–522. Okinawa, Japan: IEEE.
- Hameed, I. A., D. Bochtis, and C. Sørensen. 2011. "Driving Angle and Track Sequence Optimization for Operational Path Planning Using Genetic Algorithms." *Applied Engineering in Agriculture* 27, no. 6: 1077–1086. <https://doi.org/10.13031/2013.40615>.
- Höffmann, M., S. Patel, and C. Büskens. 2024. "Optimal Guidance Track Generation for Precision Agriculture: A Review of Coverage Path Planning Techniques." *Journal of Field Robotics* 41, no. 3: 823–844. <https://doi.org/10.1002/rob.v41.3>.
- Jensen, M. A. F., D. Bochtis, C. G. Sørensen, M. R. Blas, and K. L. Lykkegaard. 2012. "In-Field and Inter-Field Path Planning for Agricultural Transport Units." *Computers & Industrial Engineering* 63, no. 4: 1054–1061.
- Jeon, C.-W., H.-J. Kim, C. Yun, X. Han, and J. H. Kim. 2021. "Design and Validation Testing of a Complete Paddy Field-Coverage Path Planner for a Fully Autonomous Tillage Tractor." *Biosystems Engineering* 208, no. 2: 79–97. <https://doi.org/10.1016/j.biosystemsg.2021.05.008>.
- Jonnarth, A., J. Zhao, and M. Felsberg. 2023. "Learning Coverage Paths in Unknown Environments With Deep Reinforcement Learning." In *Forty-first International Conference on Machine Learning*, 1–18. Vienna, Austria: PMLR.
- Kaljaca, D., B. Vroegindeweij, and E. van Henten. 2019. "Coverage Trajectory Planning for a Bush Trimming Robot Arm." *Journal of Field Robotics* 37, no. 2: 283–308. <https://doi.org/10.1002/rob.21917>.
- Keil, J. M., and J.-R. Sack. 1985. "Minimum Decompositions of Polygona Objects." In *Machine Intelligence and Pattern Recognition*, 197–216. North-Holland: Elsevier.
- Khan, A., I. Noreen, and Z. Habib. 2017. "On Complete Coverage Path Planning Algorithms for Non-Holonomic Mobile Robots: Survey and Challenges." *Journal of Information Science and Engineering* 33, no. 1: 101–121.
- Lakshmanan, A. K., R. E. Mohan, B. Ramalingam, et al. 2020. "Complete Coverage Path Planning Using Reinforcement Learning for Tetromino Based Cleaning and Maintenance Robot." *Automation in Construction* 112, no. 12: 103078. <https://doi.org/10.1016/j.autcon.2020.103078>.
- Lee, T.-K., S.-H. Baek, S.-Y. Oh, and Y.-H. Choi. 2010. "Complete Coverage Algorithm Based on Linked Smooth Spiral Paths for Mobile Robots." In *2010 11th International Conference on Control Automation Robotics & Vision*, 609–614. Singapore: IEEE.
- Liu, H., J. Ma, and W. Huang. 2018. "Sensor-Based Complete Coverage Path Planning in Dynamic Environment for Cleaning Robot." *CAAI Transactions on Intelligence Technology* 3, no. 1: 65–72. <https://doi.org/10.1049/cit2.v3.1>.

- Luis, S. Y., D. G. Reina, and S. L. T. Marín. 2020. "A Deep Reinforcement Learning Approach for the Patrolling Problem of Water Resources Through Autonomous Surface Vehicles: The Ypacarai Lake Case." *IEEE Access* 8: 204076–204093. <https://doi.org/10.1109/Access.6287639>.
- McClure, D. E., and R. A. Vitale. 1975. "Polygonal Approximation of Plane Convex Bodies." *Journal of Mathematical Analysis and Applications* 51, no. 2: 326–358. [https://doi.org/10.1016/0022-247X\(75\)90125-0](https://doi.org/10.1016/0022-247X(75)90125-0).
- Mier, G., J. Valente, and S. de Bruin. 2023. "Fields2cover: An Open-Source Coverage Path Planning Library for Unmanned Agricultural Vehicles." *IEEE Robotics and Automation Letters* 8, no. 4: 2166–2172. <https://doi.org/10.1109/LRA.2023.3248439>.
- Nilsson, R. S., and K. Zhou. 2020a. "Decision Support Tool for Operational Planning of Field Operations." *Agronomy* 10, no. 2: 229. <https://doi.org/10.3390/agronomy10020229>.
- Nilsson, R. S., and K. Zhou. 2020b. "Method and Bench-Marking Framework for Coverage Path Planning in Arable Farming." *Biosystems Engineering* 198, no. 9: 248–265. <https://doi.org/10.1016/j.biosystemseng.2020.08.007>.
- Oksanen, T., and A. Visala. 2009. "Coverage Path Planning Algorithms for Agricultural Field Machines." *Journal of Field Robotics* 26, no. 8: 651–668. <https://doi.org/10.1002/rob.v26:8>.
- o'Rourke, J. 1998. *Computational Geometry in C*. Cambridge: Cambridge University Press.
- Piardi, L., J. Lima, A. I. Pereira, and P. Costa. 2019. "Coverage Path Planning Optimization Based on Q-learning Algorithm." *AIP Conference Proceedings* 2116: 220002.
- Pour Arab, D., M. Spisser, and C. Essert. 2023. "Complete Coverage Path Planning for Wheeled Agricultural Robots." *Journal of Field Robotics* 40, no. 6: 1460–1503. <https://doi.org/10.1002/rob.v40.6>.
- Seyyedhasani, H., and J. S. Dvorak. 2018a. "Dynamic Rerouting of a Fleet of Vehicles in Agricultural Operations Through a Dynamic Multiple Depot Vehicle Routing Problem Representation." *Biosystems Engineering* 171, no. 2: 63–77. <https://doi.org/10.1016/j.biosystemseng.2018.04.003>.
- Seyyedhasani, H., J. S. Dvorak, and E. Roemmele. 2019. "Routing Algorithm Selection for Field Coverage Planning Based on Field Shape and Fleet Size." *Computers and Electronics in Agriculture* 156: 523–529. <https://doi.org/10.1016/j.compag.2018.12.002>.
- Seyyedhasani, H., and J. S. Dvorak. 2018b. "Reducing Field Work Time Using Fleet Routing Optimization." *Biosystems Engineering* 169, no. 2: 1–10. <https://doi.org/10.1016/j.biosystemseng.2018.01.006>.
- Tan, X., L. Han, H. Gong, and Q. Wu. 2023. "Biologically Inspired Complete Coverage Path Planning Algorithm Based on Q-Learning." *Sensors* 23, no. 10: 4647. <https://doi.org/10.3390/s23104647>.
- Xu, W., C. Li, X. Wang, Y. Liu, B. Liang, and Y. Xu. 2009. "Study on Non-Holonomic Cartesian Path Planning of a Free-Floating Space Robotic System." *Advanced Robotics* 23, no. 1–2: 113–143. <https://doi.org/10.1163/156855308X392708>.
- Zhai, W., D. Wang, Z. Chen, J. Dong, X. Zhao, and C. Wu. 2021. "Autonomous Operation Path Planning Method for Unmanned Agricultural Machinery." *Transactions of the Chinese Society of Agricultural Engineering* 37, no. 16: 1–7.
- Zhang, G., C. Ji, Q. Wu, H. Liu, Y. Zhou, and J. Fu. 2022. "Study on Path Planning of Mechanized Harvesting of Ratoon Rice in the First Season Based on the Capacitated Arc Routing Problem Model." *Frontiers in Plant Science* 13: 963307. <https://doi.org/10.3389/fpls.2022.963307>.
- Zhang, M., W. Cai, and L. Pang. 2023. "Predator-Prey Reward Based Q-Learning Coverage Path Planning for Mobile Robot." *IEEE Access* 11, no. 5: 29673–29683. <https://doi.org/10.1109/ACCESS.2023.3255007>.
- Zhao, H., F. Gu, Q.-X. Huang, et al. 2016. "Connected Fermat Spirals for Layered Fabrication." *ACM Transactions on Graphics (TOG)* 35, no. 4: 1–10. <https://doi.org/10.1145/2897824.2925958>.

Zhou, K., A. L. Jensen, D. Bochtis, M. Nørremark, D. Kateris, and C. G. Sørensen. 2020. "Metric Map Generation for Autonomous Field Operations." *Agronomy* 10, no. 1: 83. <https://doi.org/10.3390/agronomy10010083>.

Zhou, K., A. L. Jensen, C. Sørensen, P. Busato, and D. Bothtis. 2014. "Agricultural Operations Planning in Fields With Multiple Obstacle Areas." *Computers and Electronics in Agriculture* 109, no. 4: 12–22. <https://doi.org/10.1016/j.compag.2014.08.013>.

Supporting Information

Additional supporting information can be found online in the Supporting Information section.